UNIVERSITÀ DEGLI STUDI DI NAPOLI
"FEDERICO II"
DIPARTIMENTO DI SCIENZE DELLA TERRA

DOTTORATO INTERNAZIONALE DI RICERCA

DINAMICA INTERNA DEI SISTEMI MAGMATICI DI VULCANI ATTIVI

CICLO XIX

"GEOCHEMICAL STUDY OF CAMPI FLEGREI ERUPTIVE PRODUCTS (FONDO RICCIO AND MINOPOLI) BY MICROTHERMOMETRY AND MICROANALYSIS IN MELT INCLUSIONS"

CANDIDATO:
Claudia Cannatelli

RELATORI:
Prof. B. De Vivo
Prof. R.J. Bodnar

ABSTRACT

Campi Flegrei is a large volcanic complex located west of the city of Naples, Italy. The area has been the site of volcanic activity for more than 60 ka and represents a potential volcanic hazard owing to the large local population. In this study, the geochemistry of the magma associated with two different eruptions at Campi Flegrei has been characterized, with the aim to identify geochemical trends that may help to predict the style and nature of future eruptions. Two eruptions of different age and eruptive style have been selected for study, Fondo Riccio (9.5 ka) and Minopoli 1 (11.1 ka). A scoria (CF-FR-C1) and a bomb (CF-FR-C2) were collected from the Fondo Riccio eruption, and two scoria samples were collected from Minopoli 1 (CF-Mi1-C1 and C2) eruption.

The pre-eruptive volatile content of magma plays an important role in the style of eruption and can be assessed from studies of melt inclusions (MI) contained in phenocrysts. Major and trace elements in Fondo Riccio MI show a wider variation compared to those in Minopoli 1 MI suggesting that the Fondo Riccio magma residence time was longer compared to the Minopoli 1 magma. Analyses of volatile contents in MI suggest that Fondo Riccio magma may have been more water-rich than Minopoli 1 magma, consistent with the more explosive character of this eruption compared to Minopoli 1. Trace element data suggest a combination of arc volcanic and upper continental crust magma as the source for the Fondo Riccio and Minopoli 1 eruptions.

ACKNOWLEDGMENTS

I would like to express my sincere gratitude to my committee members, Dr. Bob Bodnar, Dr. Benedetto De Vivo and Dr. Bob Tracy for their guidance and encouragement. Without their assistance and support, this work would not have been possible. I thank my advisor Bob Bodnar for his outstanding teaching, patience and invaluable advice. I will be always grateful for his contribution to my development as a scientist and critical thinker. I would like to thank Benedetto De Vivo for accepting me as his student at the University of Naples, Italy (even if I wasn't a geologist!) and for giving me the chance to come to the USA and work on such an interesting project! Thanks to Bob Tracy to introduce me to the wonderful (and mysterious) world of the EMPA and Dr. Annamaria Lima for her patience in helping me deal with geochemical data.

There are not enough words to explain my gratitude for Dr. Luca Fedele. He is first of all a good friend and an extraordinary colleague, and he supported me with invaluable suggestions and advice. My experimental work would not have been possible without the assistance of Charles Farley. He helped me through my innumerable crisis with the Vernadsky stage. Thanks Charles! A special thank you to the Fluid Inclusions Gang: Andras, Rocky, Tristan and Steve. Thanks for being not just an excellent group of colleagues but also and most importantly good friends! Thanks to all of the students (grads, undergrads and even Geophysicists!) and faculty of the Geosciences department for the interesting discussions, innumerable parties, field trips, fun hikes and barbeques. Thank you all for making this department such a wonderful and stimulating place to work. A special thank you to the ladies of the administrative

office, Caroline, Ellen, Linda and Mary. With their love they made me feel like I was at home. I'll be always grateful to Mrs. Connie Lowe. She paved the way of becoming a VT student and if I receive this degree is because of this wonderful woman who supported me during the past two years. I would like to thank my family and friends in Italy, for their love, encouragement and support. Last but certainly not least, I thank my parents. They have always left me the freedom to follow my dreams, even when this meant moving overseas!! They always believed in me, I would not be here and be what I am without them. Mamma e papa', grazie infinitamente!!!

TABLE OF CONTENTS

Cap. 1

INTRODUCTION

The geochemical evolution of an active volcanic system and identification of the parameters that play a role in determining the style of an eruption are of fundamental importance to understand the past behavior of a magmatic system and to forecast future behavior. Development of geochemical models for volcanic eruption forecasting require information on the volatile content of the magma before an eruption, because volatiles play a major role in controlling the nature and style of eruptive events (Anderson, 1976; Burnham, 1979). The exsolution and expansion of volatiles (especially H_2O) provides the mechanical energy that drives explosive volcanic eruptions. The original volatile content of magma can be estimated by analyzing melt inclusions (MI) contained in phenocrysts (Anderson, 1974; Clocchiatti, 1975; Roedder, 1979; Belkin et al., 1985; Sobolev, 1990; Lowenstern, 1994; Anderson, 2003; Wallace, 2005). Moreover, MI may provide information concerning crystallization and mixing histories of magmas and also the conditions of primary melt generation and extraction (Roedder, 1984; Carroll and Holloway, 1994; Lowenstern, 1994; Sobolev, 1996; Marianelli et al., 1999; Danyushevsky et al., 2000; Frezzotti, 2001).

The Campi Flegrei volcanic complex is an active volcanic field in the Neapolitan area (Italy) that has experienced predominantly explosive volcanic activity for more than 60,000 years. The city of Pozzuoli lies close to the Solfatara crater (actually it was built on the deposits of numerous eruptions of the past 10 ka) while Naples, with 1.5 million inhabitants, is nearby, between Campi Flegrei and Vesuvius. The volcanic risk in this area is significant because of the large

population and is a compelling reason to better understand the evolution of the Campi Flegrei complex and the mechanisms that lead to explosive eruptions. We studied the products of two eruptions that occurred in Campi Flegrei during the First Cycle: Fondo Riccio (9.5-10.3 ka) and Minopoli 1 (10.3-11.5 ka). Fondo Riccio was an explosive strombolian eruption that occurred near the center of the Campi Flegrei caldera, whereas Minopoli was an explosive hydromagmatic eruption that occurred along the regional fault system in the northern portion of the Campi Flegrei caldera. Data from MI were used to constrain the evolution of major and volatile (H_2O, Cl, S and F) element concentrations, with the goal to reconstruct the crystallization history of the magmas and assess pre-eruptive volatile abundances for the two eruptions.

Cap. 2

CAMPI FLEGREI (PHLEGRAEAN FIELDS)

2.1 Tectonic Setting

The Campanian Province, the southernmost sector of the Plio-Quaternary volcanic belt along the Italian peninsula, is formed by the active volcanoes Somma-Vesuvius, Ischia and Campi Flegrei (Phlegraean Fields) and by the islands of Procida and Vivara (Fig.2.1). Sometimes the Pontine islands (Ponza, Palmarola, Zannone, Ventotene and Santo Stefano) are included in the Campanian Province even if petrological data suggest that just Ventotene, Santo Stefano and the youngest rocks of Ponza (1 Ma) have similar composition with those from Campanian Volcanoes.

The volcanic centers of the Campanian Province developed in Quaternary extensional basins along the Tyrrhenian Sea border at the intersection between NE-SW and NW-SE fault systems. The Pontine Islands form a row of volcanoes (W-E trend) along the 41st parallel tectonic Line (Serri 1990; Bruno et al., 2000). The thickness of the lithosphere along this transect varies from about 50km along the Tyrrhenian Sea border to more than 110 km in the Apulia foreland. The depth

of Moho has a range between 20-25 km offshore the Tyrrhenian Sea cost, 40km beneath the central zone of the Apennine chain and 30km beneath the Apulia foreland (Piromallo and Morelli, 2003).

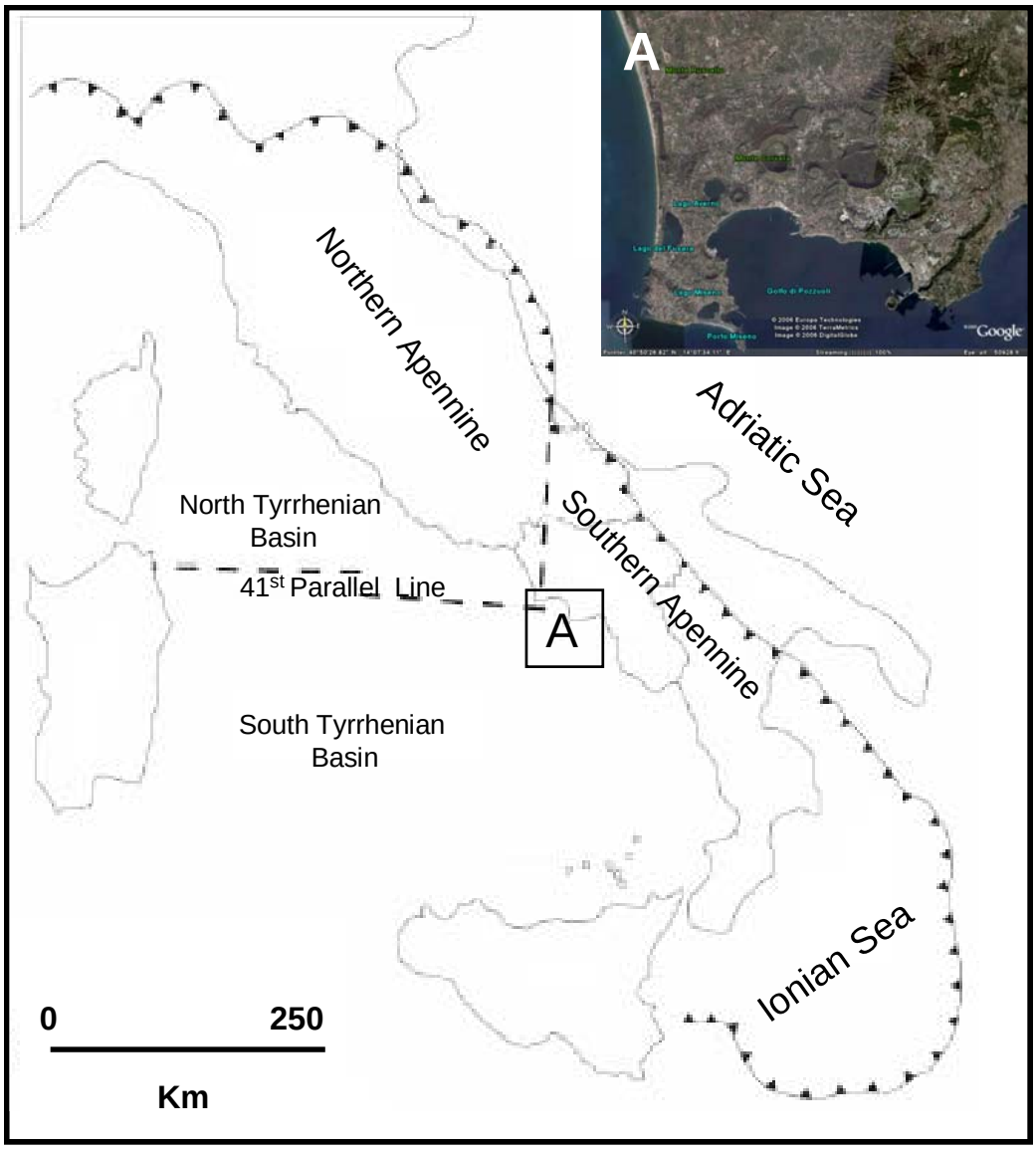

Fig. 2.1 *Schematic tectonic map of Italy showing the main tectonic blocks. The box A outlines the region of the Campi Flegrei volcanic complex shown in the enlargement. (A) map of Campi Flegrei (by Google Earth).*

The area between the Campanian Province and Vulture (located east of the Apennine chain on the western border of the Apulia foreland) is characterized by a moderate elevation and positive Bouguer anomaly, which crosses the Apennines from Tyrrhenian sea to Apulia. Such a lineament is sited along the continuation of 41st Parallel Line which divides the northern and southern section of the Tyrrhenian basin (Bruno et al, 2000).

The Campi Flegrei Volcanic District lies in the Campanian Plain (CP), between the western side of the Southern Apennine Chain and the eastern border of the Tyrrhenian abyssal plain. Since late Miocene-early Pliocene, the Tyrrhenian Sea has been opening (Scandone, 1979; Doglioni, 1991) and the Calabrian arc has migrated to the SE following rollback of the subducted Ionian plate under Calabria (Selvaggi and Chiarabba, 1995; Piromallo and Morelli, 1997; Gvirtzman and Nur, 2000), as shown in Fig.2.2. Extension in the Tyrrhenian basin was accompanied by contemporaneous compression in the Apennine chain (Meletti et al., 2000). As a result of motions of the Tyrrhenian and Ionian blocks, the CP became a structural depression bordered by NW-SE and NE-SW trending faults (D'Argenio et al., 1973; Ippolito et al., 1975; Hippolyte et al., 1994). Geological, geophysical and petrologic evidence (Selvaggi and Amato, 1992; Serri et al., 1993; Peccerillo, 1999) suggest that subduction of oceanic lithosphere (from the relict Ionian basin) beneath the Apennines occurred concomitant with thinning of the continental lithosphere in the region of the Adriatic Sea, Sicily and North Africa.

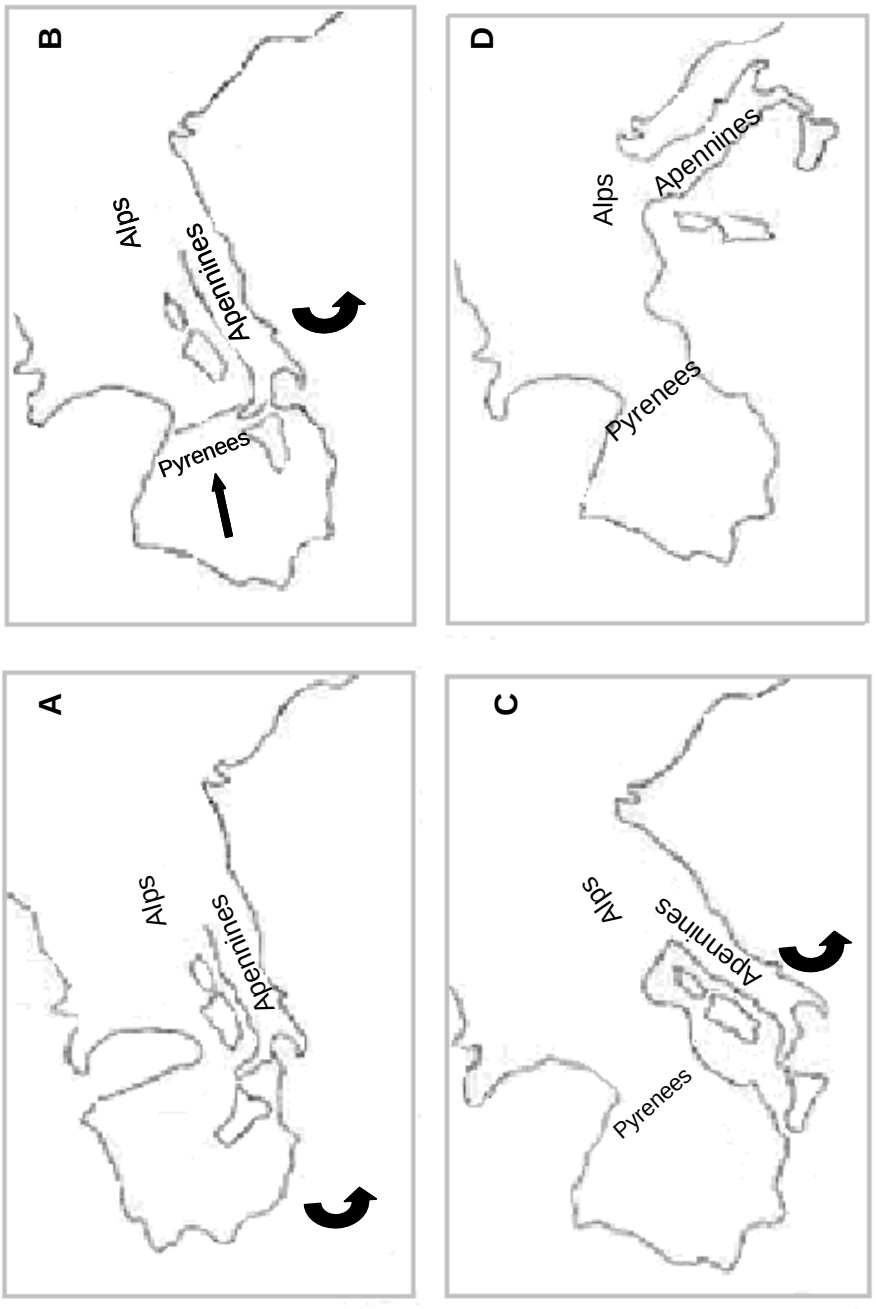

Fig.2.2 *Schematic representation of the rotation of the Italian Peninsula.* ***(A)*** *65 Ma;* ***(B)*** *46 Ma;* ***(C) 15*** *Ma;* ***(D)*** *0 Ma.*

2.2 Volcanic Setting

The Campi Flegrei caldera (Fig, 2.3) is one of the most active volcanic systems in the Mediterranean region. The area is known for intense hydrothermal activity, frequent earthquakes and bradyseismic events that occurred between 1969-1972 and 1982-1984.

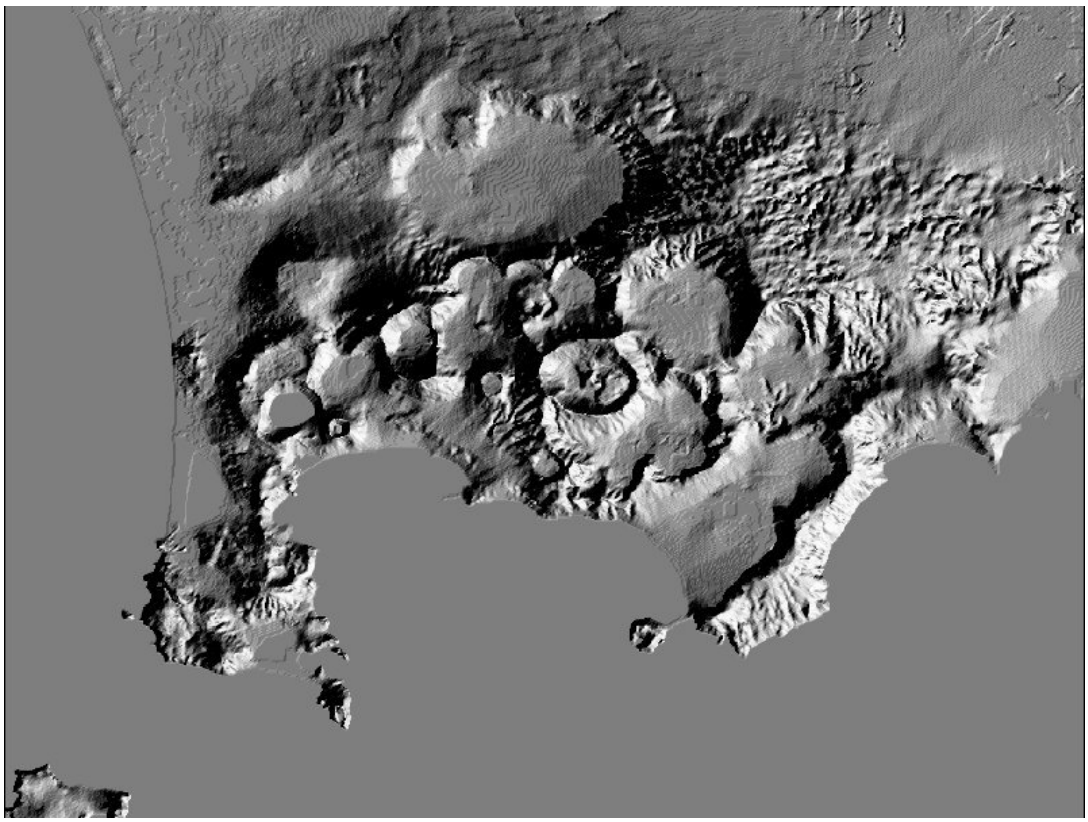

Fig. 2.3 *DEM (Digital Elevation Model) of Campi Flegrei volcanic complex.*

The area has been volcanically active for 60 ka (Pappalardo et al., 2002) and many studies have been devoted to understanding its activity (Di Girolamo et al., 1984; Rosi and Sbrana, 1987; Barberi et al., 1991; Pappalardo et al., 1999; De Vivo et al., 2001; Rolandi et al., 2003). At Campi Flegrei, numerous eruptions from multiple sources have produced lava and pyroclastic deposits (Fig. 2.4), including several lava dome structures. Some authors (Rosi and Sbrana, 1987; Orsi et al., 1996) relate the origin of Campi Flegrei either to the eruption of the Campanian Ignimbrite (CI) (39 ka, De Vivo et al., 2001), or to the Neapolitan Yellow Tuff (NYT) (15 ka, Deino et al., 2004). An interpretation that considers the eruption of the CI to be a unique event originating in the Campi Flegrei caldera has been questioned by De Vivo et al. (2001) and Rolandi et al. (2003). These authors describe a sequence of eruptive events from fractures activated along the neotectonic Apennine fault system parallel to the Tyrrhenian coastline. These events, of ignimbritic origin, lasted from >300 ka to 19 ka and are not confined to a unique volcanic center in Campi Flegrei (Rosi and Sbrana, 1987; Orsi et al., 1996). Only the Neapolitan Yellow Tuff (NYT) (15ka, Deino et al., 2004) erupted within Campi Flegrei, whereas the CI (39 ka, De vivo et al., 2001) has a much wider source area (Rolandi et al., 2003). According to Pappalardo et al. (2002), the time between the CI and NYT eruptions is characterized by a large number of significantly less powerful events. Volcanism in this interval is poorly defined, primarily because of limited exposure due to cover by younger deposits, restriction to submarine exposure, and intense urbanization. Since the NYT eruption the edge of the caldera has been the site of at least 65 eruptions during three periods of activity (15.0–9.5; 8.6–8.2; and 4.8–3.8 ka), as shown in Fig. 2.5.

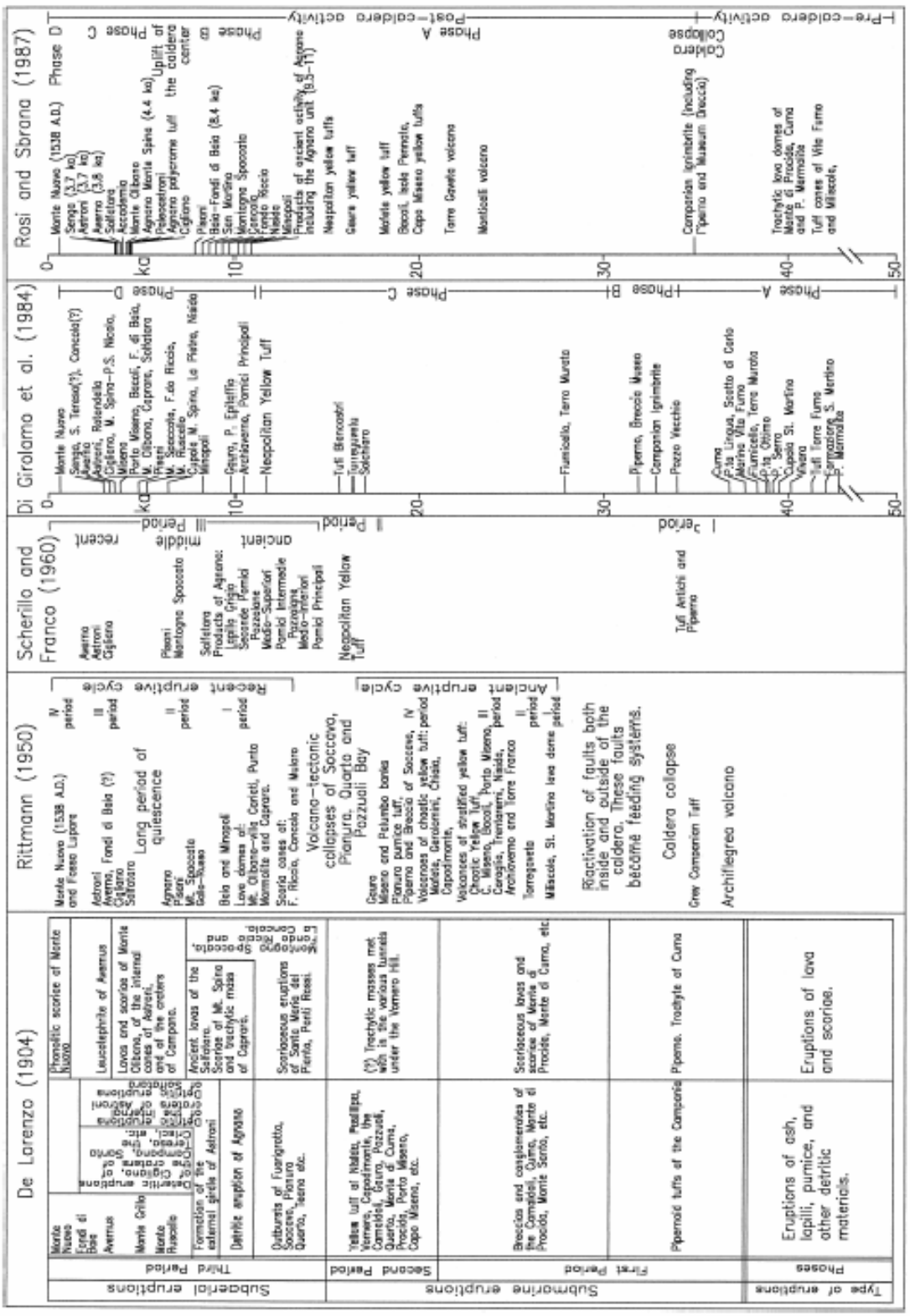

Fig. 2.4 *Chronostratigraphy of the volcanic activity in Campi Flegrei (Di Vito et al., 1999).*

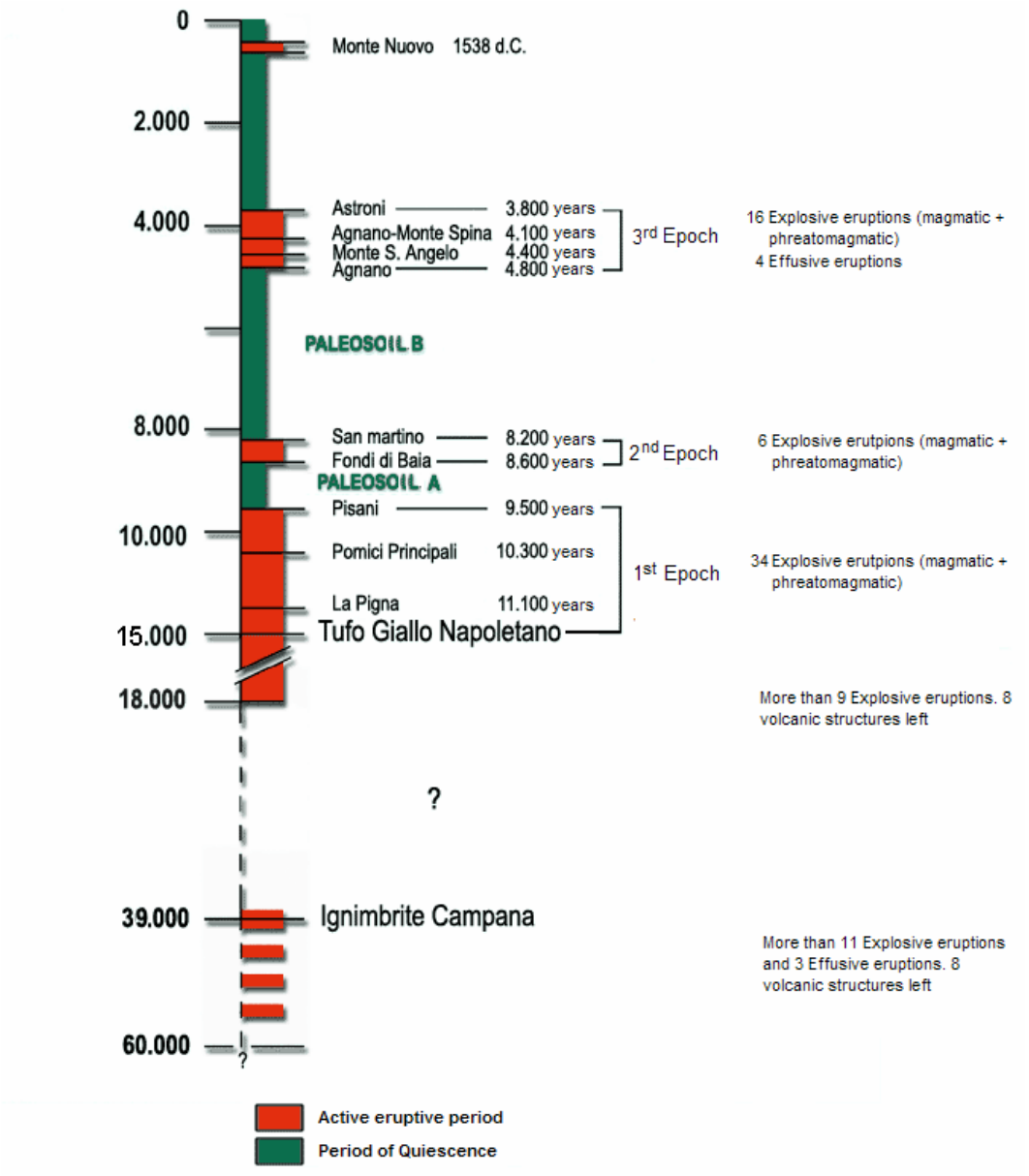

Fig. 2.5 *Chronology of the volcanic activity in Campi Flegrei (modified from http:/www.ov.ingv.it/)*

These eruptions were separated by quiescent periods marked by two widespread paleosoils (Di Vito et al., 1999). During each eruptive period, eruptions were separated by short-time intervals, on the order of tens of years. The last eruption in 1538 formed the Monte Nuovo cone (Di Vito et al., 1987) after 3.4 ka of quiescence .

Campi Flegrei eruptions were mostly explosive with variable degrees of magma/water interaction; only a few events were effusive. The volcanic products range from trachybasalt to alkali-trachyte and phono-trachyte, and are characterized by variable Sr-Nd-Pb-B isotope ratios (D'Antonio et al., 1999a; Pappalardo et al., 2002; Tonarini et al., 2004) and involve different magma types (i.e. from different sources and/or with different history) or source processes.

2.3 Bradyseismic Events

Several theories were formulated regarding the dynamic of eruptions in Campi Flegrei area, but they are all based on limited evidence. The only eruption occurred in ancient period at Campi Flegrei described by contemporary reporters is the eruption that generated Monte Nuovo, a little volcanic cone with elevation of 150 m near Pozzuoli. We know that Monte Nuovo represents one of the minor events of the eruptive history of Campi Flegrei, consisting in the eruption of a relatively small volume of magma (about 25 millions of m^3). Reading contemporary chronicles it is possible to assess the existence of remarkable bradiseismic events during the period before the eruption.

At the beginning of XVI century the area between Baia and Pozzuoli developed a progressive elevation, evidenced by the migration of the coast line. This bradiseismic phenomenon is confirmed by several seismic events occurred two years before the eruption of 1538 A.D. First interpretations of bradiseismic events were in 1792, when some scientists started to study the traces of marine organisms on the Roman column of Serapide Temple, the ancient market of Roman Age, near the Port of Pozzuoli (Fig. 2.6). From that moment the variation of the sea level in Serapide Temple and in general of bradiseismic phenomena were interpreted in various ways. A good description is given by Parascandola (1947), where the author reconstructed the variations of level in Serapeo Temple relatively to the last 2000 years sea level. The reconstructed trend shows a general subsidence starting from the eruption of Monte Nuovo.

In the last 30 years bradiseism at Campi Flegrei made often the news, because of an abrupt inversion of ground movement, characterized by two episodes of fast uplift occurred within a decade from one another. The first of this episodes occurred between 1970 and 1972 when the ground, accompanied by several earthquakes, raised about 70 cm in the Port of Pozzuoli.

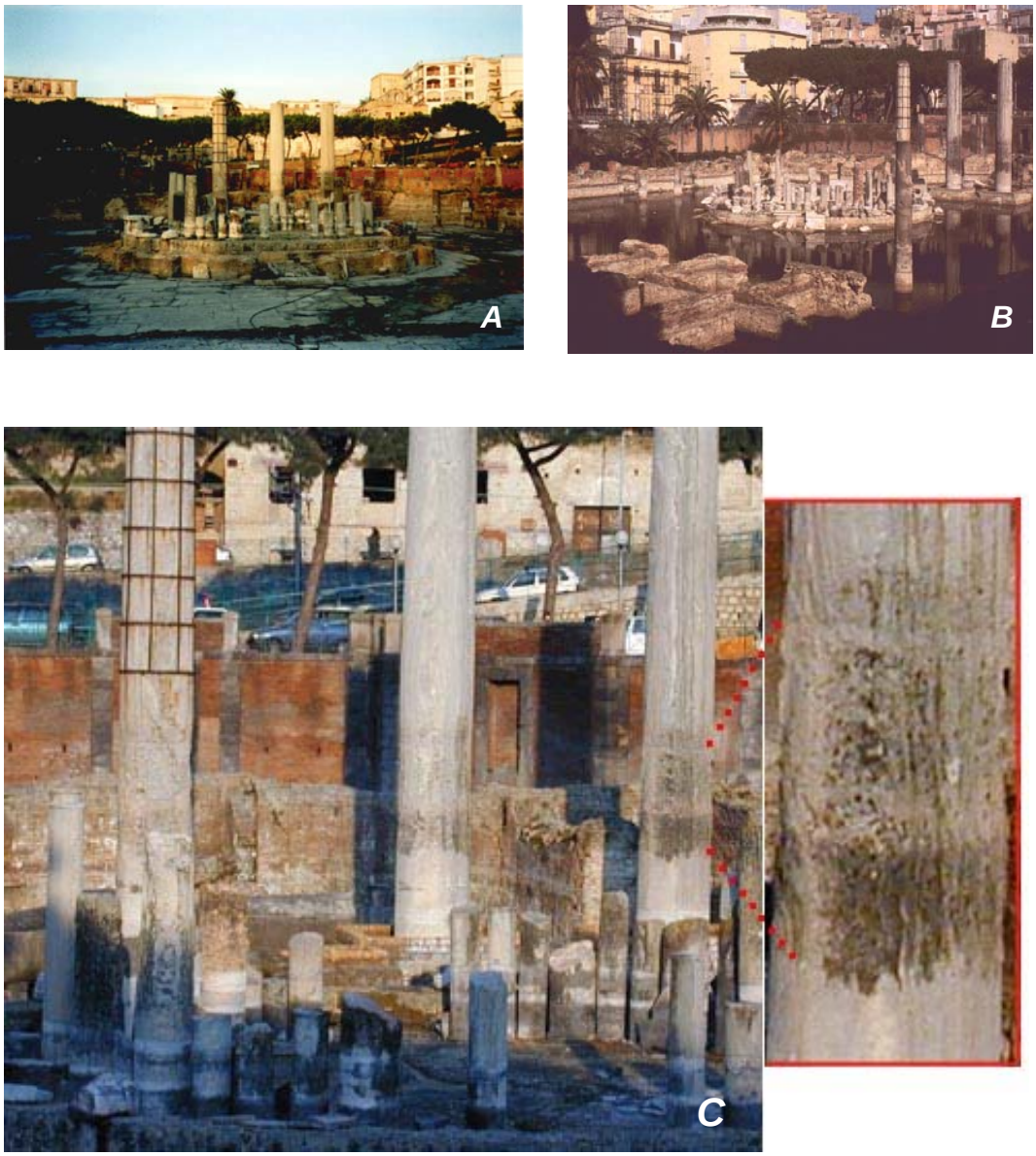

Fig. 2.6 *Serapide Temple, Pozzuoli. A-B) It is easy to observe the difference of the water level due to a phase of deflation of the ground. C) Traces of marine organisms on the Roman column of Serapide Temple.*

The most important episode occurred between 1982 and 1984 when a very fast uplift of the ground level was recorded (Fig. 2.7); this level didn't change in the previous ten years but showed only few oscillations. The ground uplift started during summer 1982 and continued with a mean velocity of about 6 cm every month (but it pikes of 0.5 cm per day were recorded) until 1984, when the total uplift reached the value of 1.80 m. During the autumn of 1984 uplift velocity decreased, and at the end of that year inflation ended and a new phase of deflation started which continues today. Uplift episodes are also characterized by horizontal deformations whose value is approximately equal to the half of vertical uplift.

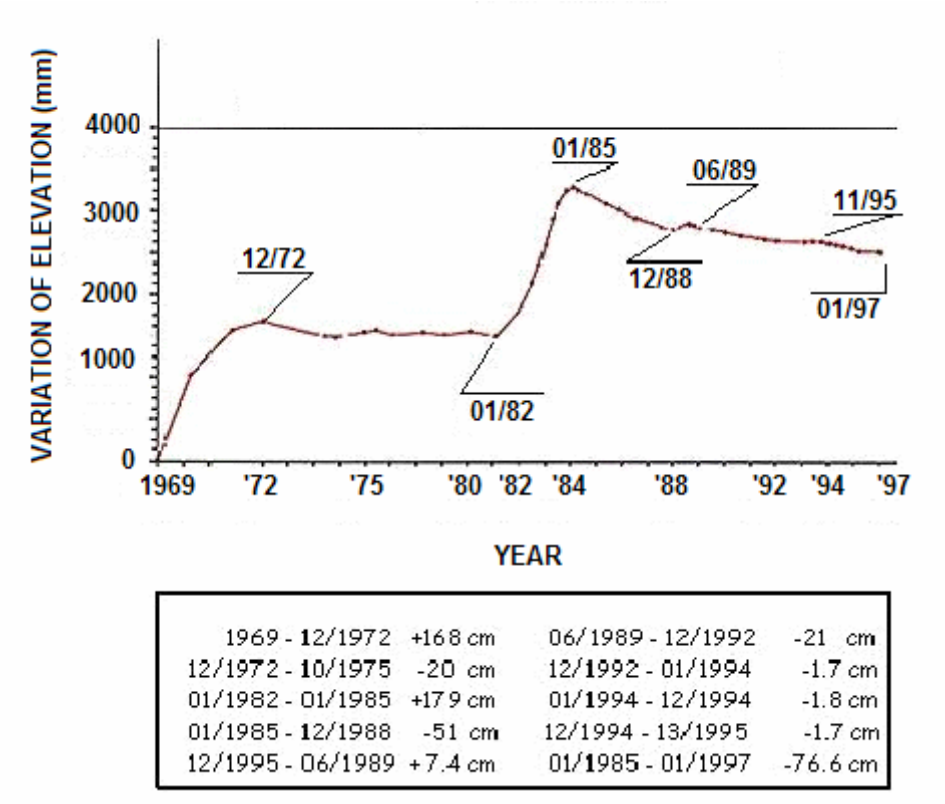

1969 - 12/1972	+168 cm	06/1989 - 12/1992	-21 cm
12/1972 - 10/1975	-20 cm	12/1992 - 01/1994	-1.7 cm
01/1982 - 01/1985	+179 cm	01/1994 - 12/1994	-1.8 cm
01/1985 - 12/1988	-51 cm	12/1994 - 13/1995	-1.7 cm
12/1995 - 06/1989	+7.4 cm	01/1985 - 01/1997	-76.6 cm

Fig. 2.7 *Variation of elevation (in mm) measured at datum point number 25, in Pozzuoli. In the table it is showed the amount of deformation (in cm) for each observed period.*

Ground deformations in volcanic areas are generated by the rising of the pressure of the rocks at a certain depths; the expansion source depth is determined by the amplitude of deformed area. Ground deformations in Campi Flegrei, limited to a circular zone with radius from Pozzuoli less than 3 km, showed a source centre at a depth of 2-3 km.

In this area proposed causes for the deformations are: 1) the migration of hot flows under pressure (Oliveri del Castillo e Quagliariello, 1969; Casertano et al., 1976; Oliveri del Castillo e Montagna, 1984); 2) overpressure in a magmatic chamber (Corrado et al., 1977; Berrino et al., 1984; Bonafede et al., 1986; Bianchi et al., 1987); 3) overpressure of the magmatic chamber and heat convective transfer to confined superficial aquifers (Bonafede, 1990; De Natale et al., 1991).

The latter hypothesis is supported by De Vivo et al. (1989, personal communication) who suggest that ground deformations could be generated by the heating of the aquifers overlying the magmatic chamber. Heated fluids would remain under lithostatic pressure for long periods and the heat, supplied by continuous input of magma, could determine overpressure in the upper area confined by impermeable rocks, causing uplift of overlying rocks (positive bradisism). A crisis would occur with a change from lithostatic to hydrostatic pressure, with consequent boiling, hydraulic fracturing, volcanic tremor and then pressure release. At this point the area would experience maximum rising, then followed by pressure release and beginning of subsidence. Afterward the system, saturated with boiling fluids, begins to seal again. The beginning of a new positive bradisism phase will occur only after several years when the system “reloads” with new lithostatic pressure. Ground deformations and the seismicity are associated with the presence of intense fumarolic and hydrothermal activity, concentrated in the crater of Solfatara where CO_2 and H_2O fluxes are particularly intense and probably originated by a magmatic degassing system (Chiodini et al., 2001).

Cap. 3

MELT INCLUSIONS

3.1 What are they?

Silicate-melt inclusions (MI) are small droplets (in volcanic rocks usually >50 μm) of silicate melt containing some combination of crystals, glass and vapor entrapped in different minerals during their growth. They can form at high pressure and temperatures and are contained within relatively incompressible phenocrysts, so they retain high concentrations of volatile elements that normally escape from magma during the degassing. For this reason they represent a unique chance to reconstruct the chemical composition of magma at a specific stage of its evolution. After trapping of MI, these Microsystems closed and evolved independently from the host minerals and the enclosing lava. MI have been studied for nearly 150 years, although most of the early studies were simply descriptive, with little or no interpretations of their significance in terms of geological processes. During this same period, a parallel but much more intensive study was under way of aqueous inclusions. In contrast with the study of MI, the aqueous inclusions studies almost immediately began to yield data on many geological and economically important processes (temperature of hydrothermal ore-formations, compositions of fluids actively involved in many environments). Similar studies of MI can in theory yield similar information of nature, origin and evolution of the fluid (melt) that was trapped and the process that took place in the past. The two areas of research that have been most fruitful are:

a) stable isotopes (especially O, C, S, B, Cl , etc.)
b) the volatiles.

For a better understanding of the next paragraphs, the following table summarize some of the key concepts about Melt and Fluid Inclusions:

MELT INCLUSIONS (MI)	Contains glass or crystallized glass.
FLUID INCLUSIONS (FI)	Contains one or more fluids at T_{room} and no glass
VAPOR-RICH FI	FI with >50 vol % bubble at T_{room}; i.e., low density fluid.
MIXED INCLUSIONS	More than one magmatic phase trapped.
HYDROSALINE MELT	Molten solution of salts and H_2O

The study of MI allows researchers to have information about dissolved volatile concentrations in magmas (H_2O, CO_2, Cl, S, F, B, Li), the minimum pressure of crystallization, the approximate temperature during crystallization, the existence and the approximate composition of coexisting exsolved fluids. They are also important to investigate about the process of magma mixing and the existence of a time scale of magmatism/volcanism. It is not possible to obtain from the study of MI any information about the composition of bulk magma, the maximum pressure of entrapment (and therefore depth) and the role of magma in the formation of epithermal ore deposits.

3.2 History of MI

In his pioneering detailed study, Sorby (1858) gave rigorous descriptions and drawings of MI and FI (Fig. 3.1) in a wide variety of intrusive and extrusive rocks. He speculated on the origin of the bubbles within the inclusions and recognized that MI had marked promise for interpretations of the origin of igneous rocks. He was among the first to recognize that the coexistence of MI and FI is synonymous of entrapment in a volatile-saturated magma. For a variety of reasons, decades would pass before other worker followed Sorby and studied MI in igneous phenocrysts. The first modern studies of MI were undertaken in ’60, ’70, ’80, by workers interested primarily in the systematic of FI in the field of economic geology (Roedder).

At this time the international FI community championed the use of MI for studies of lunar samples (Roedder and Weiblen 1970, 1971), pegmatites, granoitoids and volcanic rocks (Sobolev and Kostyuk, 1975; Roedder 1979).

The apparent low impact of MI studies on the volcanological and petrologic communities can be related to the uncertainty of MI as truly representative of the composition of the host magmas. In 1995 Eichelberg said: “Interpretations of melt inclusions is not without difficulties: 10^{-14}g samples are taken to represent 10^{10} g systems.....”.

Roedder (1979, 1984) gave a thorough discussion of MI, their origins, the methods of study and work and more recently (1992) the information which melt inclusions provide on magmatic immiscibility processes. In 1993 Touret & Frezzotti describe the study techniques of MI in granitic rocks and the information they can provide in plutonic environments.

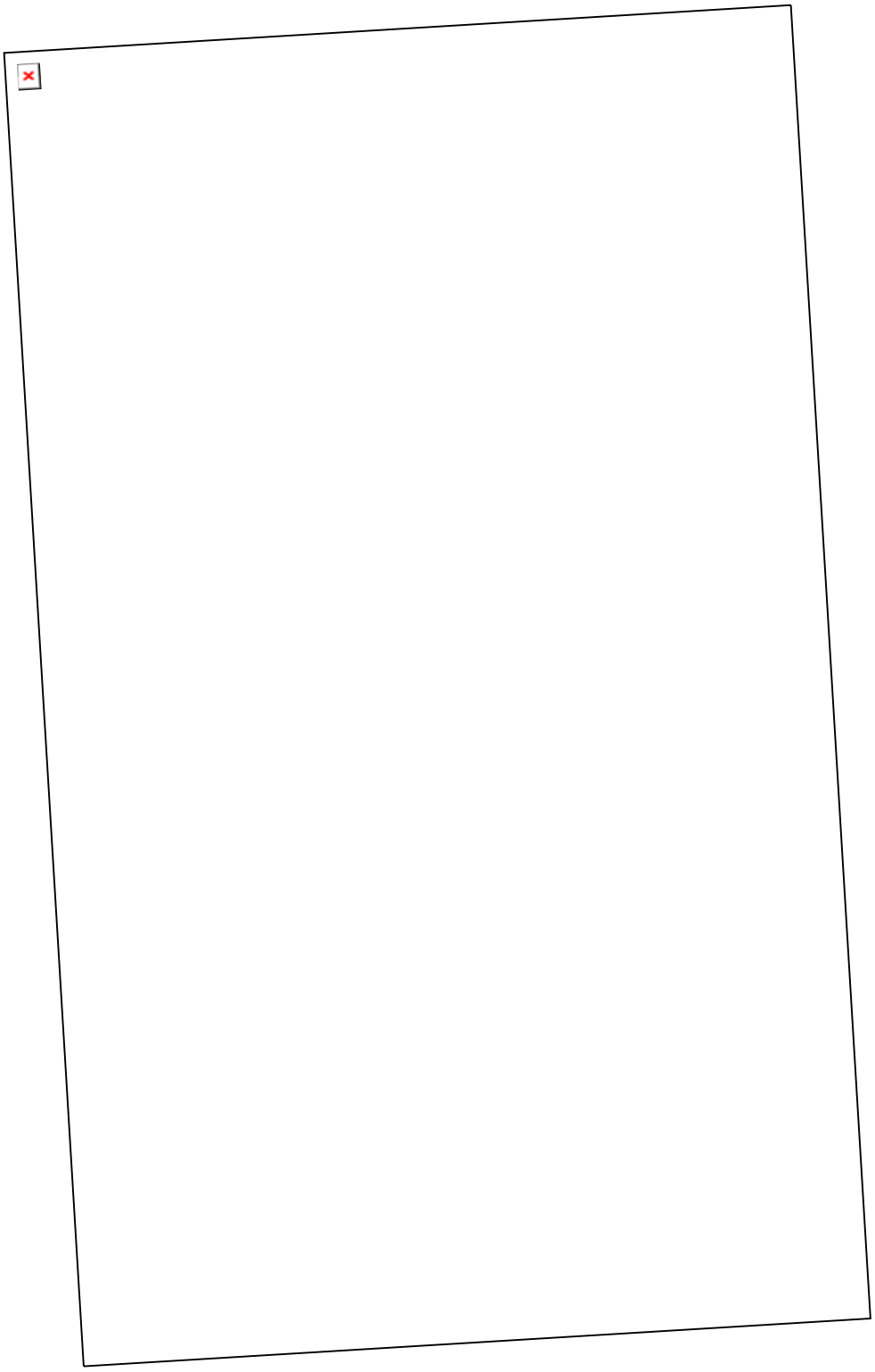

Fig. 3.1 *Original drawings of silicate-melt inclusions in effusive and intrusive rocks by Sorby (1858).*

In 1994 Johnson et al., discussed about the information MI provide about the pre-eruptive volatile contents of four magmatic systems: Kilauea, Mt. S. Helens, the Bishop Tuff and Mt. Pinatubo. Bodnar (1995), Kamenetsky et al (1999), Davidson & Kamenetsky (2001) discussed and analyzed the melt-volatile immiscibility process in porphyry copper deposits. The reviews by Lowenstern (1995, 2003), Sobolev (1996) and Wallace (2005), focused on the applications of silicate-melt inclusions for the study of magmatic volatiles and on the formation mechanisms of silicate-melt inclusions, gave further details about the study techniques.

In the last decade improvements in analytical methods and careful studies of MI systematics made scientists more convinced of the utility of these features to explain the complexities of volcanic systems. The reliance on MI has come only after several decades of concerted effort to improve analytical techniques, to assess the reliability of MI due to host-inclusion equilibration (pre-, syn- or post-trapping), and to recognize the effects of trapping multiple fluid phases. Additional effort has been placed on characterization of bubbles within MI, which can be present for a variety of very different reasons.

Using microbeam analysis of the quenched MI, scientist were able to quantify the pre-eruptive concentrations of dissolved volatile gases (i.e., H_2O, CO_2, S, and Cl), they can estimate the formation pressures of melt-vapor equilibration (Anderson et al., 1989). Studies of MI also allow workers to recognize that elements such as B, P, and F have higher concentrations in MI than degassed matrix glass. Studies of ore metals such as Cu, Zn and Sn show that they also can be transported as volatiles in magmatic systems. The reliance on MI has come only after several decades of concerted effort to improve analytical techniques, to assess the reliability of MI due to host-inclusion equilibration (pre-, syn- or post-trapping), and to recognize the effects of trapping multiple fluid phases. Additional effort has been placed on characterization of bubbles within MI, which can be present for a variety of very different reasons.

Only within the past 10-15 years volcanologists and petrologists have regularly accepted MI utility for characterizing magmatic systems. Their relatively slow acceptance was due to several reasons: 1) Lack of reliable

analytical techniques; 2) Concern that MI could represent anomalous boundary-layer melts or could be affected by leakage or post-entrapment crystallization; 3) Data sets indicative of heterogeneous melts; 4) Homogenization temperatures greater than those calculated by other techniques.

Much of the work on MI focused on traditional homogenization experiments, primarily to assess magmatic temperatures, developing several experimentally based geothermometers. The temperatures found from MI homogenization studies were in general greater than those inferred by analysis of coexisting Fe-Ti oxides. Roedder (1979b) suggested several reasons for high homogenization temperatures, such as slow diffusion of melt components, thermal gradients in the stage, diffusive loss of H_2 or H_2O. Recent studies have verified that homogenization studies can provide uncertain data because of diffusion of volatiles through the host and stretching of the phenocryst container during laboratory experiments at atmospheric pressure (Massare et al., 2002). Another uncertainty in the acceptance of MI studies was the large variation in apparent volatile concentrations in MI from some eruptive units. There are a number of geological reasons that can result in a spread of H_2O concentrations in MI from volcanic phenocrysts from a single unit. Potential explanation for this variation of volatiles can be related to magma mixing, crystal settling, degassing-induced crystallization and lava drain back and recycling. Another possibility is that MI can decrepitate and leak during or after eruptive ascent and scientists have to be careful to avoid that leaked/degassed inclusions.

Another important barrier to widespread use of melt inclusions was the lack of micro-analytical techniques, and the exploding development of high-precision bulk techniques. In the 1980s, techniques such as x-ray fluorescence (XRF) and instrumental neutron-activation analysis (INAA) spurred a revolution in trace element geochemistry of whole rocks. Lots of improvements in mass spectrometers allowed researchers to focus on isotopic studies of terrestrial and planetary samples. The new data were interpreted in light of recently developed plate-tectonic theory and recognition that different magma types and environments had their unique trace element and isotopic characteristics. Until the 1990s, MI could not be analyzed reliably for trace elements, and analysis of

volatile elements was qualitative therefore volcanologists chose not to use MI to understand petrogenesis and volcanic phenomena.

It had long been recognized that magmatic volatiles had a crucial role in the generation, ascent and crystallization of magmas (Bowen, 1928). Until 1980s a variety of high profile experimental studies were undertaken to determine the thermodynamic controls on volatile solubilities (Burnham and Jahns, 1962; Burnham and Davis, 1971; Eggler and Burnham, 1973; Wyllie, 1979; Whitney, 1984). Many workers suggested that data on natural samples could not be properly understood without an experimental and thermodynamic basis for interpretation. In natural samples, volatile concentrations were estimated by bulk analytical techniques on lavas quenched at the surface or underwater. H_2O fugacity was later estimated by thermodynamic models and the pressure of H_2O was believed to be far below total pressure in most igneous systems. Many scientists concluded that most crustal magmas were water and vapour undersaturated, because of the absence of high abundances of other volatiles (CO_2, SO_2, H_2, N_2, Cl-bearing species.

Nowadays, MI are used as a volcanological tool to unravel the complexities of very recent eruptions. Dunbar et al. (1989) undertook one of the first studies to use the ion microprobe to quantify H_2O in MI. Roggensack et al. (1997) studied the degassing history of eruptions from Cerro Negro (Nicaragua) finding that magmas erupted explosively in 1992 had equilibrated at greater depths than lavas erupted three years later as effusive lavas. Shallow subsurface degassing led to the decrease in explosivity. In a subsequent paper Roggensack (2001a) looked at the products of an 1867 eruption at Cerro Negro and found that MI glass composition and gas saturation pressures correlated with crystal size, implying that large crystals grew at greater depth (up to >15 km). Similar studies on Italian volcanoes demonstrate the importance of degassing and crystallization in determining eruptive style. Métrich et al. (2001) looked at crystal-rich scoria at Stromboli (erupted during mild strombolian activity) and found that the MI are degassed and contain more evolved glass than MI from compositionally equivalent whole-rocks erupted as crystal-poor pumices during more energetic explosive activity. They suggested that volatile-rich magma batches can either

ascend rapidly to produce the explosive eruptions, or they can intrude to shallow depths and degas quietly to spur the typical strombolian eruptions. These orts of studies provide new opportunities for evaluating the relationship between crystal growth, ascent rate, degassing and eruptive style. Besides these volcanological studies, petrologists have increasingly used MI to understand magma generation and the diversity of melt sources available to volcanic systems (Sobolev, 1996; Frezzotti, 2001). A recent compilation (Hauri et al., 2002) provides an excellent assembly of papers on MI systematics and analysis, primarily focussed on the petrology of mafic magma systems. The petrological and volcanological communities have become familiar with MI analysis and have accepted them as a very powerful tool to understand magmatic systems.

3.3 Classification of MI

The common terminology for categorizing aqueous or carbonic fluid inclusions cannot be easily applied to silicate MI hosted in volcanic rocks.. For example, most non-silicate FI are described by Roedder (1984) as:

1) primary;
2) secondary;
3) pseudo secondary.

Primary inclusions contain any phase present at the time of crystal growth. Secondary inclusions contain phases that enter crystals along fractures (after primary crystal growth has ceased) and then are trapped as the fractures heal. Pseudo secondary inclusions are also trapped along fractures, but before the crystal has ceased growing at its periphery. Most igneous petrologists suggest that both primary and pseudo secondary MI are "primary" in the sense that they are trapped within growing crystals and yield information on the composition of the silicate liquid during its evolution. Under some circumstances (such as magma mixing), there may be more than one primary melt from which the host crystal grew. It is difficult to envision how secondary MI may be trapped in volcanic phenocrysts (because of the high viscosity of silicate melts), though Pasteris et al. (1996) convincingly showed how non-silicate fluids can be trapped as secondary inclusions, particularly during fracturing events associated with magma ascent. Metasomatic secondary MI are commonly described in xenoliths found in volcanic ejecta (Schiano et al. 1994) and can potentially form in plutonic environments if a silicate melt infiltrates a previously crystallized rock. Several studies have been conducted about the formation of crystallized MI (Roedder 1979, 1984, Lowenstern 1995, Frezzotti, 2001). It has been noted that for a given inclusion size, the slower the cooling rate, the more likely the melt in the inclusions will crystallize. Furthermore, for a given cooling rate, the bigger the inclusion, the faster it will crystallize respect to a small one. Roedder (1984) and

Student & Bodnar (1999) noted that in addition to cooling rate and inclusions size, the composition of the melt can affect the crystallization process. In particular these authors suggest that the high H_2O content of the melts and the fact that during trapping the melt was saturated in water, might have promoted crystallization during cooling.

One of the most important aspects of a MI or FI study is determining which inclusion to study and whether these inclusions are representative of the physical and chemical conditions at the time of trapping. It is important to constrain the time of the trapping of an inclusion relative to the formation of the host phase, as well as the position of the host in the overall paragenesis. In 1975 Sobolev and Kostyuk summarized the different temporal occurrence of MI during magmatic crystallization. They distinguish between zonal and azonal primary MI. Zonal inclusions define a growth zone and are common in minerals like plagioclase, nepheline and pyroxene, but less common in olivine. Azonal inclusions are isolated and randomly distributed and are not associated with a specific growth feature.

Within the FI community has been developed a procedure that allows researchers to select inclusions and be confident with the obtained results. This procedure consists in identifying a group of FI that are all trapped at the same time, temperature and pressure and from fluids of the same composition. This group of inclusions is called Fluid Inclusions Assemblage (Goldstein and Reynolds, 1994) or FIA and is the most finely discriminated trapping event that can be identified on petrography. Because similar petrographic techniques are required to study MI, similarly a Melt Inclusions Assemblage, or MIA has to be chosen. MIA represents a group of MI trapped at the same time, temperature and pressure and from a melt of the same composition. In volcanic rocks, MI consist of glass ± one or more gas bubbles ± daughter mineral phases (Fig.3.2a). The size of the bubble is important because it depends mainly on cooling behavior, melt composition and volatile content of the inclusion. In general in volatile-poor melts, a single shrinkage bubble can be observed and some inclusions contain only glass (Fig.3.2b), while in volatile-rich melts, fluids under pressure may be

present within the bubble. It is sometimes difficult to detect these fluids because of their low density.

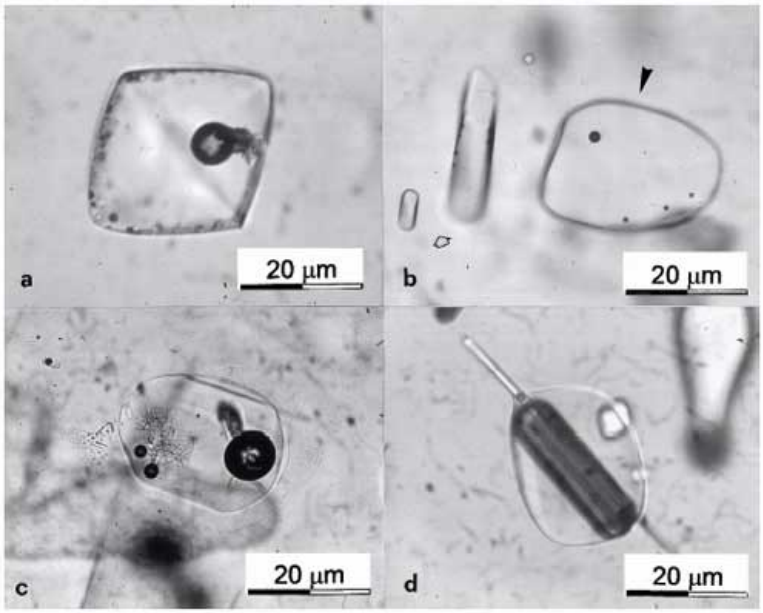

Fig.3.2 *Examples of MI in volcanic rocks. a) MI consist of glass ± one or more gas bubbles ± daughter mineral phases; b) MI with a single little shrinkage bubble (volatile-poor melts); c) MI with one big shrinkage bubble and two small bubble (volatile-rich melts);d) MI with a solid inclusion (www.dst.unisi.it/geofluids-lab/).*

If the magma is volatile-rich, the trapped MI will contain a large bubble at Troom, composed by vacuum and gas (Fig. 3.2c). The formation of primary MI is in general related to irregularities in crystal growth, such as defects of growth due to different processes (undercooling, stagnation, kinking), wetting by an immiscible fluid phase, or trapping of solid inclusions (Fig. 3.2d). These irregularities of growth may control the distribution of inclusions within a single crystal (Fig. 3.3) In a b-quartz crystal (Fig. 3.3a and 3.3b) the preferential distribution of melt inclusions is in the {1120} faces; in olivine and pyroxene crystals the tendency is to trap inclusions in a more random way (Fig. 3.3c); in plagioclase MI fare trapped along the growth zones of the crystal (Fig. 3.3d).

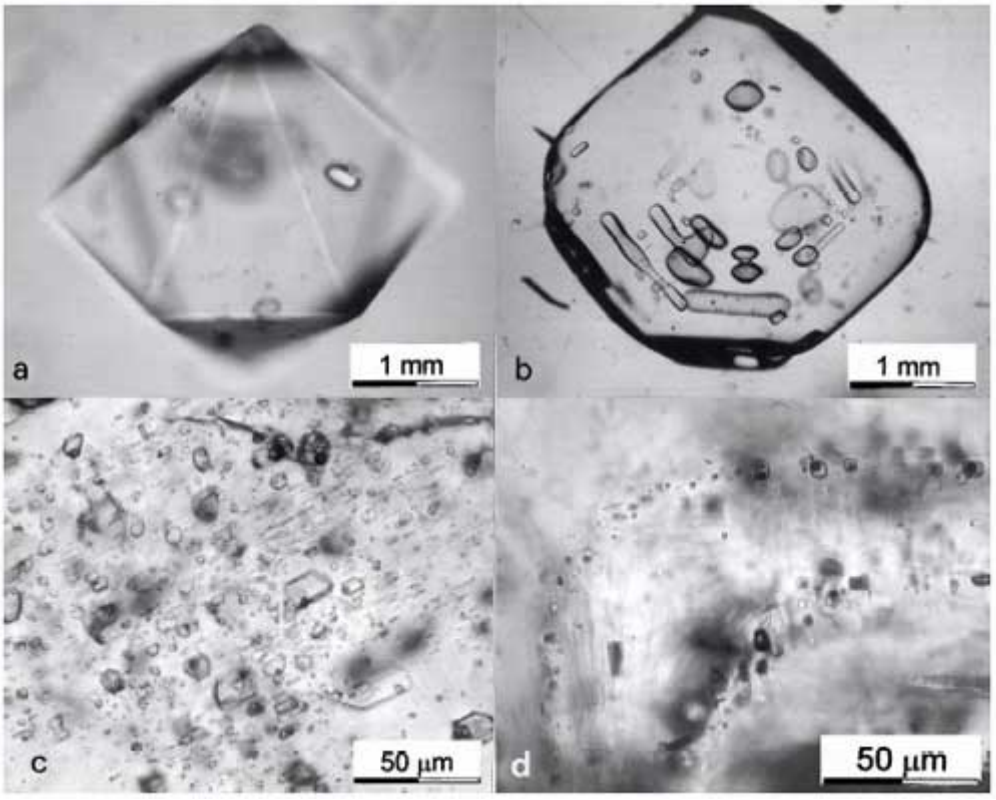

Fig. 3.3 *Irregularities of growth of the host crystal control the distribution of MI. a-b) Quartz; c) Pyroxene; d) Feldspar (www.dst.unisi.it/geofluids-lab/).*

A variation in temperature and/or X_{H2O} or mixing processes have an important role in the formation of melt inclusions in plagioclase. The resulting inclusion shapes can vary, having very often smooth morphologies and following the symmetry of the host mineral phases. Similarly to FI, regularly shaped inclusions, for example negative crystals, can be the result of re-equilibration processes between host mineral and the inclusions.

Many researchers have avoided the study of bubbles, or inclusions containing bubbles, to simplify interpretation of MI compositions. However bubbles, with their size, composition and distribution can reveal the history of fluid immiscibility, degassing and ascent rate of the host magma. A bubble can be found within a MI for several reasons:

1) it can be formed during near-constant-volume cooling of homogenous silicate melt;

2) it can be formed during decrepitation/leakage of the MI;

3) it can represents magmatic vapor that was co-trapped with melt in a mixed inclusion.

Similarly with FI, a bubble can nucleate due to isochoric (constant volume) cooling of a trapped homogeneous liquid, causing depressurization and resultant saturation with a low-density phase. The bubble that forms is often called a "shrinkage bubble" and Roedder (1984) suggested to considered it as a separate phase formed by immiscibility of the melt and vapor. Typically, such bubbles appear empty, or at least without a liquid phase, allowing H_2O pressures no greater than that for liquid saturation at 25°C ($2.6x10^{-3}$ MPa). Some workers interpret the empty bubbles to reflect extreme hydration of the glass adjacent to the bubble rim during cooling of the MI (Lowenstern, 1995). The volume of bubbles have a wide range, from 0.1 to 5 vol.% and depends on the cooling history of the MI. Small MI often don't have bubbles because of surface-tension effects (Roedder, 1979b). Many studies have shown that MI from rapidly quenched Plinian pumice often lack bubbles entirely (Clocchiatti, 1972; Sommer, 1977; Beddoe-Stephens et al., 1983), also confirmed by both theoretical and experimental studies. In intrusions, crystallization of the melt at near-magmatic temperatures will allow the MI-hosted bubbles to reach as much as 15-20 % of the total inclusion volume (Student and Bodnar, 1996).

When the host crystal cools more slowly the bubble has time to form, causing the internal pressure of the MI to rise. Often these slowly cooled rocks contain cracked crystals with MI that contain numerous large bubbles (Lowenstern, 1995; Best and Christiansen, 1997) that can often be attributed to the decrepitation of MI during eruption. Infact, MI partially or fully decrepitated, are likely to have numerous large bubbles and degassed. Anderson (1991) defined another category of leaked MI, called "hourglass", which consist of glass or crystallized melt connected to the outside of the host crystal by a canal or capillary that at magmatic temperatures allows the melt to be expelled from such inclusions.

The entrapment of FI or mixed inclusions in igneous phenocrysts is a clear evidence for the presence of vapors or other non-silicate fluids. In intrusive rocks it is common to observe vapor-rich FI trapped contemporaneously with (and separately from) silicate melt (Roedder, 1984, 1992; Frezzotti, 1992; Touret and Frezzoti, 1993; Lowenstern et al., 1997; Audétat et al., 2000; Dietrich et al., 2000; Frezzotti, 2001). Such inclusions are rare in volcanic rocks, which instead contained silicate MI. Reasons for the absence vapor-rich FI in the crystals within volcanic rocks have been discussed by Anderson (1991) who concluded that any MI with a trapped vapor bubble would create a pressure gradient during magma ascent, preventing the inclusion from sealing. Tait (1992) suggested that MI with co-trapped vapor are more likely to break during the eruption. Another explanation is that small bubbles are rare in long-lived magma chambers, and bubbles are unlikely to be trapped within sub-cm-sized crystals. As the magma becomes crystal-rich and the liquid is closer to saturation with a pure-H_2O vapor, small bubbles may nucleate and would be trapped more commonly.

Cap. 4

TECHNIQUES

4.1 Preparation of the samples for heating experiments

Doubly polished thin sections 30μm - 1.5mm thick were prepared from all samples, with the thickness varying as a function of phenocryst size and clarity. Sections were examined petrographically, and those samples containing recognizable and useable melt inclusions were selected for further study. The selected samples were washed in distilled water and then dried in vacuum conditions at 100° C. The rocks were then crushed and sieved (10 and 20 mesh) and phenocrysts (pyroxene, plagioclase, and olivine) that were hand picked under a binocular microscope. For each sample, about 50-60 crystals for each mineral phase were hand picked. Phenocrysts removed by crushing were mounted on glass slides, ground to produce a flat surface and then polished. The phenocrysts were then removed from the slide and remounted with the polished side down, and the second side was ground and polished to produce doubly polished wafers ranging from 30μm to 1.5mm thick. Once the phenocrysts were polished both sides, the slide was placed in acetone for 12-24 hours to remove the crystals from the slide.

4.2 Heating experiments

All the inclusions examined in this study consisted of a heterogeneous mixture of crystals and/or glass plus a volatile phase. In order to produce a homogeneous glass for microbeam analyses, it was necessary to heat the inclusions to melt the crystalline phases and dissolve the volatiles back into melt (homogenization). Then the melt was rapidly cooled to form a homogeneous glass. The main factor that complicated homogenization of melt inclusions was the decrepitation of volatile-rich melt inclusions during heating. The two methods for melt inclusion homogenization that were utilized and evaluated in the course of this study are:

1) heating in a microscope heating stage;
2) heating in a 1 atmosphere vertical tube furnace.

The main advantage of studying melt inclusions in doubly polished wafers is that inclusions can be observed not only before and after, but also during heating (Danyushevsky et al., 2002). Also, MI may trap solid phases along with the melt, and if these solids are incorporated back into the melt during heating, a wide range in melt compositions would result, with the variability being a function of the relative size of the trapped solid phases. If the inclusions are not observed before and during heating, the heterogeneous nature of the inclusions would not be recognized and the resultant range in MI compositions might be incorrectly interpreted to be the result of petrogenetic processes. In order to observe the melting behavior of the inclusions, we used microscope-mounted heating stages with slow heating rates.

We selected 3 crystals-bearing MI for each mineral phase present in each sample and we heated them in order to homogenise the MI. Crystal-bearing melt inclusions in quartz phenocrysts were initially heated on a Vernadsky Stage (Sobolev et al., 1980), designed to flow He gas (that had been deoxygenated by

passing through a tube of powdered Ti metal heated to 600°C) over the sample, thus preventing oxidation and darkening of iron-bearing phases. The stage was mounted on a Leitz petrographic microscope equipped with a 20x-long working-distance objective (Fig. 4.1). After homogenization the power was turned off and the temperature decreased several hundred degrees in the first few seconds.

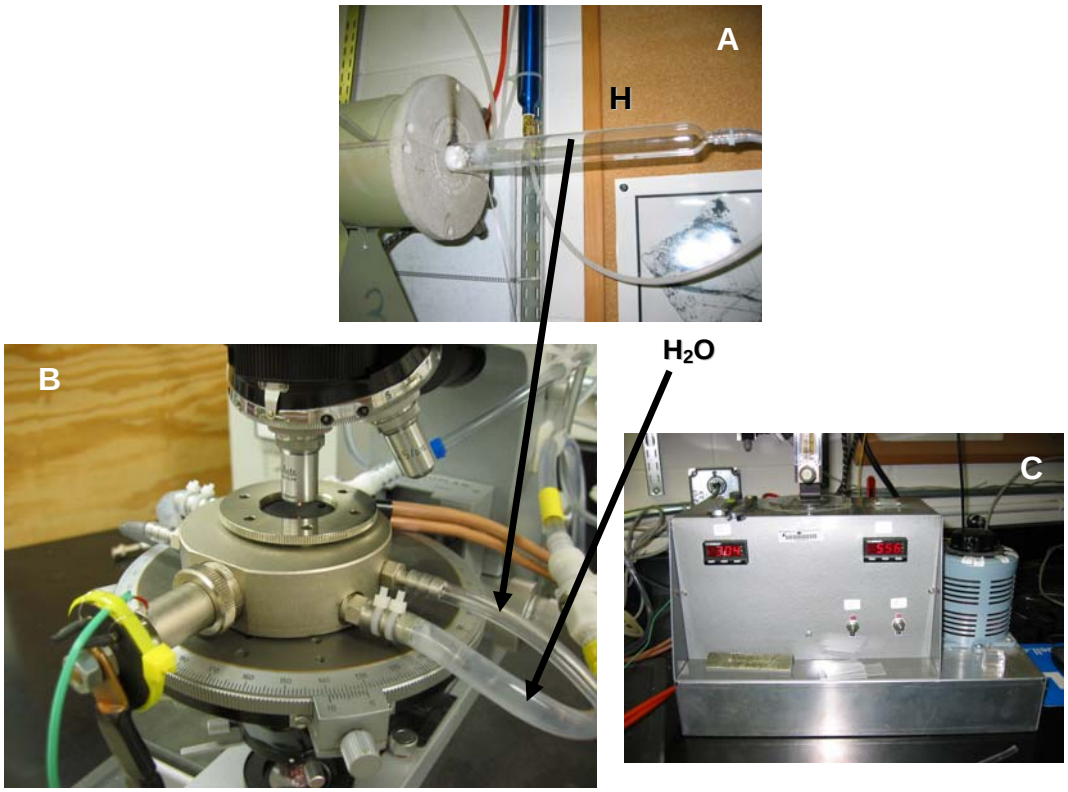

Fig. 4.1 *Vernadsky Stage. (A) Tube of powdered Ti metal passing in the furnace heated at 600°C; (B) Stage; (C) Central control and variac (on the right) to regulate the intensity of power (and therefore the heat).*

All the experiments were conducted in controlled (inert gas) atmosphere to avoid oxidation of the crystal according to the procedure described in Danyushevsky et al. (2000) and Lima (2000). The precision of temperature measurements is ± 3ºC at 1200ºC (measured by thermocouple), based on calibration using known melting points of Ag (938º C) and Au (1064ºC).

Once we conducted these preliminary experiments, we had an idea of the homogeneization temperatures of MI in each mineral phase in each sample. Therefore we use the vertical furnace to speed up the homogenization procedure. A group of crystals-bearing MI was incrementally-heated in a 1-atmosphere vertical tube furnace. The crystals were placed in a Pt foil with a drop of oil, inserted in a capsule and suspended from the top of the furnace trough a Platinum wire (Fig. 4.2). The sample was positioned within the "hot-spot" of the furnace, where previous tests had determined a thermal gradient of ± 5°C over a distance of ± 8 cm from the centre of the "hot spot".

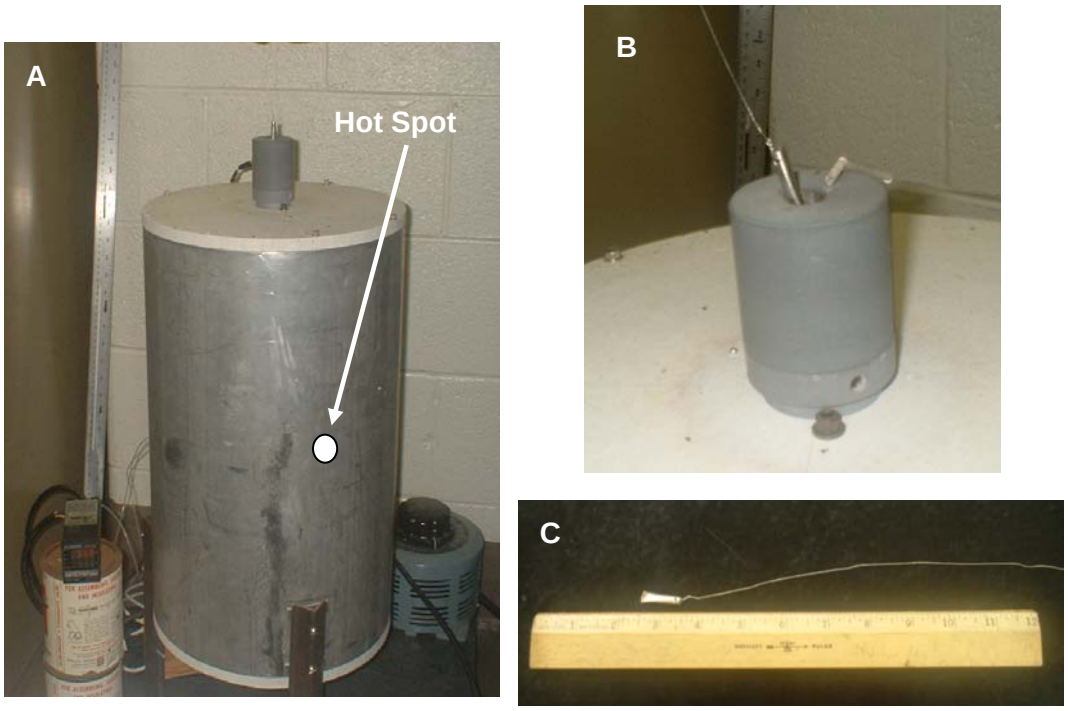

Fig. 4.2 *Vertical Furnace. (A) "Hot spot". (B) Detail of the inserting of the capsule; (C) Platinum capsule and the Pt wire.*

The furnace thermocouple was calibrated using pure silver at 961°C, and at lower temperatures this thermocouple was calibrated against another well-calibrated thermocouple. The accuracy and precision of temperature measurements at 800°C is estimated at ± 10°C.

3.3 Preparation of the samples for EMP and SIMS analyses

After homogenizing the inclusions, host phenocrysts were ground and polished by hand to expose homogenized melt inclusions for Electron and Ion microprobe analysis. Phenocrysts were polished and prepared for analyses following the procedure described in Thomas and Bodnar (2002), mounting crystals on polycarbonate rods.

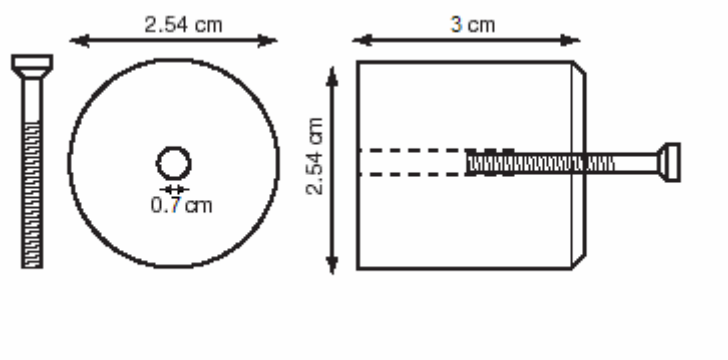

Fig. 4.3 *Drawing of the polishing tool, adjusting screw for mounting crystals.*

To mount the crystal to the epoxy tipped rods, a small droplet of crazy glue is placed on the pre-flattened surface and spread to the appropriate thickness (thinner than the crystal to be mounted) with a dissecting needle. This thin layer of crazy glue fixes the crystal to the surface prior to the final application of epoxy. Using a binocular microscope, a single crystal is placed onto the end of the rod containing the thin layer of crazy glue, and a final drop of epoxy is added to cover the crystal. Epoxy should be mixed and allowed to react for ~30 min prior to application.

After curing, the rods are placed into the polishing tool (Fig. 4.3) and ground with 1200 grit polishing paper and water. Grinding progress is monitored through repeated grinding and observation under a binocular microscope using reflected light until the crystal is exposed on the surface. After exposing the crystal surface, the rod is removed from the polisher and observed under a petrographic microscope using both transmitted and reflected light. The rod acts as an optical fiber and transmits light to the crystal. If the desired level within the crystal is reached, it is necessary to achieve a final polishing using 0.3 mm aluminum oxide-coated polyester film and water. The rods are positioned in a stainless steel holder (4 rods for each holder) until sets of samples are ready for EMP and SIMS analysis (Fig. 4.4).

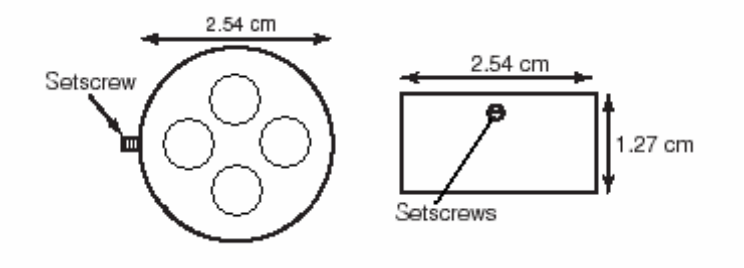

Fig. 4.4 *Drawing of the electron microprobe mount containing rods with polished crystals.*

4.4 Electron Microprobe

EPMA (or Electron Probe Micro Analysis) can probe a specimen as small as 5 microns, and not only identify the elements present but measure them with a small degree of error. These instrument represent a great advances in scientific instrumentation, however it does have limits. For example, not all specimens can be exposed to the high vacuum within the specimen chamber. Also, elements lighter than atomic number 8 (oxygen) can not be measured without reservations, and EPMA is not sensitive to many elements below 100 ppm. Materials are bombarded with accelerated electrons with high energies. Our microprobe, on the other hand, is designed with its *wave* The heart of EPM is the wave dispersive technology (WDX) for detecting and counting x-rays. These spectrometers are much more sensitive to low elemental concentrations than are EDX detectors usually associated with SEM. Concentrations in the range of 500-1000 ppm can generally be measured, and for some elements within some types of materials, the detection limit can be near 20 ppm.

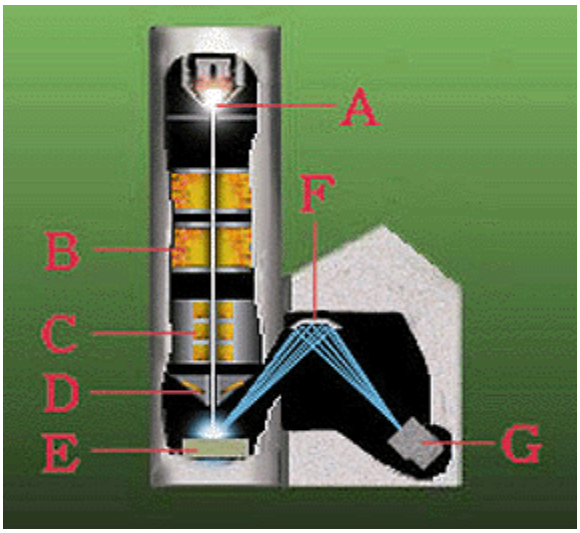

Fig. 4.5 *Scheme of an EMPA. (A) Filament; (B) beam; (C) Aberrations; (D) focused beam; (E) sample; (F) reflectant crystal; (G) detector.*

Electrons are produced by heating a filament similar to the filament in a light bulb (Fig.4.5A). These electrons are then formed into a beam by accelerating them down a column at very high voltages, typically 15 to 20 thousand volts. The electrons pass through lenses that condense the beam (Fig.4.5B), remove aberrations (Fig.4.5C) and focus the beam (Fig.4.5D). When the electrons arrive at the sample (Fig.4.5E) the beam is focused into a spot much smaller than 0.001 millimeter in diameter. Upon entering the sample, the electrons interact with the atoms in the sample in what is called the interaction volume, causing X-rays to be produced. Each element produces X-rays with characteristic energies. These X-rays can then be counted by reflecting them through a crystal (Fig.4.5F) and sending them on to a detector (Fig.4.5G). By counting the X-rays generated by each element in the sample and comparing that number to the number of X-ray generated by a standard of known composition, it is possible to determine the chemical composition of a spot one one-thousandth of a millimeter in diameter with great accuracy.

Quantitative electron microprobe analyses (EMPA) were performed at Virginia Tech and at University of Rome "La Sapienza" (IGAG-CNR, Rome, Italy) on a Cameca SX50 equipped with four wavelength dispersive spectrometers (Fig.4.6). The analytical schemes was chosen for major/minor oxide analyses. Analysis of SiO_2, TiO_2, Al_2O_3, FeO, MnO_2, MgO, CaO, Na_2O, K_2O, NiO, Cr_2O_3, P_2O_5, and Cl, S and F and standardization were preformed using silicate, oxide, phosphate and glass standards, and the data were corrected with the PAP method, developed by Pichou and Pouchoir (1985), using vendor supplied software. Analyses were performed at 15kV, using a current of 20nA with a defocused beam diameter of 10 μm and counting time 10 seconds, as recommended by Morgan and London (1996). Relative one-sigma precision is estimated to be 1 to 2 % for major elements and 5 to 10 % for minor elements. In each analytical run, alkalis were counted first, and no correction has been made for Na loss. Test runs made prior to the beginning of the analysis on synthetic and natural glass standards of known composition showed no significant alkali migration under the specified analytical conditions.

Fig.4.6 *Electron Microprobe Cameca SX/50 (Virginia Tech).*

Two points were analyzed in larger MI, whereas only one point was analyzed in smaller inclusions (<10μm). When no significant difference in composition was detected, an average of the two analyses was used. If the two analyses were significantly different the results were discarded. If just one spot was possible, a comparison between the obtained data and data for other MI in the same sample was made to test for consistency. Note, however, that two or more analyses were obtained on ~90% of the MI. Host phenocrysts were analyzed at distances of about 20 μm from MI with accelerating voltage of 15kV and beam current of 20 nA.

The analytical sequence and counting times on 4 spectrometers were:

spectrometer 1 (TAP) Na_2O; Al_2O_3; P_2O_5 and MnO.
spectrometer 2 (PET) MgO; SiO_2 ; K_2O and Cr_2O_3.
spectrometer 3 (PET) F ; TiO_2 and NiO.
spectrometer 4 (LIF) FeO; CaO; Cl and S.

Standards were analyzed at 15 kV, using a current of 20nA with 10 μm rastered beam.

4.5 SIMS (Secondary Ion Mass Spectroscopy)

The technique of Secondary Ion Mass Spectrometry (SIMS) is the most sensitive of all the commonly-employed surface analytical techniques because of the inherent sensitivity associated with mass spectrometric-based techniques. In SIMS the surface of the sample is subjected to bombardment by high energy ions; this leads to the ejection (or sputtering) of both neutral and charged (+/-) species from the surface. The ejected species may include atoms, clusters of atoms and molecular fragments. In traditional SIMS it is only the positive ions that are mass analysed, primarily for practical ease but it does lead to problems to quantify the compositional data since the positive ions are but a small, non-representative fraction of the total sputtered species. Furthermore the displaced ions have to be energy filtered before they are mass analysed (i.e. only ions with kinetic energies within a limited range are mass analysed). The most commonly employed incident ions used for bombarding the sample are argon ions (Ar^+) but other ions (e.g. alkali metal ions, Ga^+) are preferred for some applications. The mass analyser is typically a quadrupole MS analyser with unit mass resolution, but high specification time-of-flight (TOF) analysers are also used and provide substantially higher sensitivity and a much greater mass range (albeit at a higher cost). A simplified synoptic of the original IMS 3f design is shown in Fig. 4.7. primary ions, usually O^- or O_2^-, are produced in a duoplasmatron ion source (DP) and extracted into the primary column through potenzials of 12.5 kV. A pair of Einzel-type electrostatic lenses is used to focused the primary ions to a small diameter spot on the sample surface. Simple four plate deflectors are used to center the primary ion beam through these lenses.

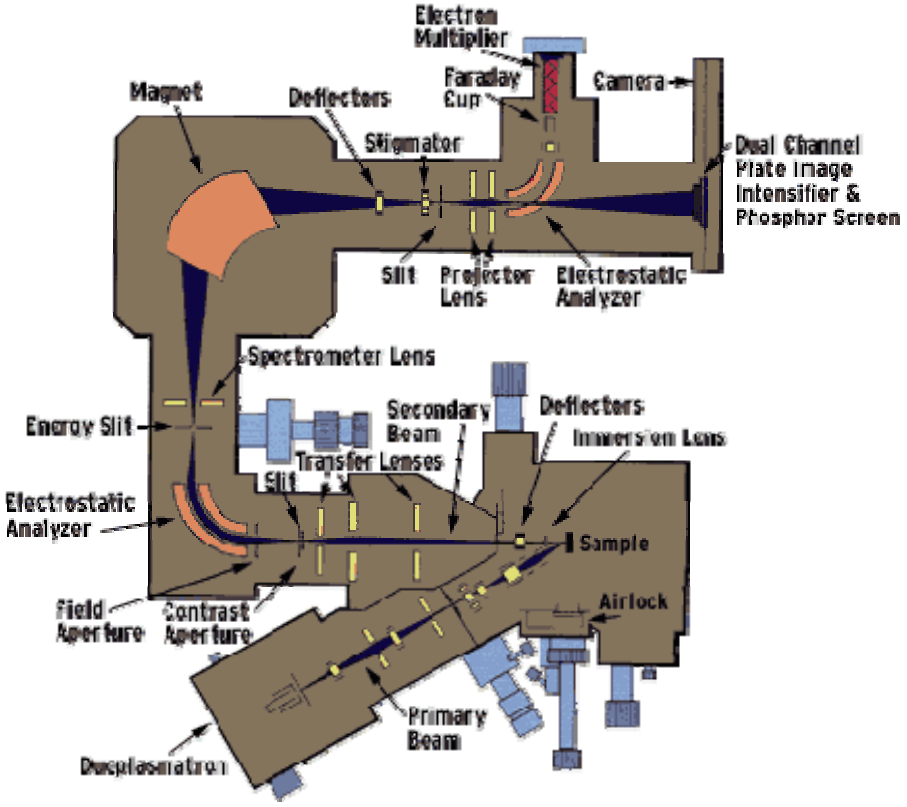

Fig.4.7 *Simplified synoptic of the original IMS 3f design.*

The deflector plates can also be enabled to deliver a square-rastered primary beam to the sample, or to deflect it into a faraday cup to measure the primary current. An eight palte stigmator is also associated with the deflector and and enables further shaping of the beam. The instrument also uses a double focusing (Nier-type) mass spectrometer, which accommodates energy filtering and modest mass resolution to eliminate isobaric interferences.

Selected MI were analyzed for H (reported as H_2O), Li, Be, B, Rb, Sr, Y, Zr, Nb, Cs, Ce, Sm, Dm, Yb, Th and U by Secondary Ion mass Spectrometry (SIMS) at the Woods Hole Oceanographic Institution (Fig.4.8), using techniques detailed by Shimizu and Hart (1982) and Webster et al. (1996). Accelerating potential was 10kV and beam current was 1-2 nA. The inclusions were analyzed in one spot, five times each in depth profile mode. Precision and accuracy were monitored with NBS (National Bureau of Standards) reference glasses NBS 610.

Results on the NBS glasses are similar and within 5% of the accepted values; H_2O concentrations are reproducible to $\pm$ 0.3 to 0.4 wt% and trace elements to 5 to 15% (for more details see Webster et al., 2001).

Fig. 4.8 *Cameca IMS 3f, Woods Hole Oceanographic Institution (WHOI) in Woods Hole, Massachusetts, USA.*

4.6 Raman Spectroscopy

Raman spectroscopy is based upon the Raman effect which is described as the scattering of light from a gas, liquid or solid with a shift in wavelength from that of the usually monochromatic incident radiation. When a transparent medium was irradiated with an intense source of monochromatic light, and the scattered radiation was examined spectroscopically, not only is light of the exciting frequency, ν_0, observed (Rayleigh scattering), but also some weaker bands of shifted frequency are detected. Moreover, while most of the shifted bands are of lower frequency $\nu_0 - \nu_i$, there are some at higher frequency, $\nu_0 + \nu_i$. By analogy to fluorescence spectrometry, the former are called Stokes bands and the latter anti-Stokes bands. The Stokes and anti-Stokes bands are equally displaced about the Rayleigh band; however, the intensity of the anti-Stokes bands is much weaker than the Stokes bands and they are seldom observed (Fig. 4.9).

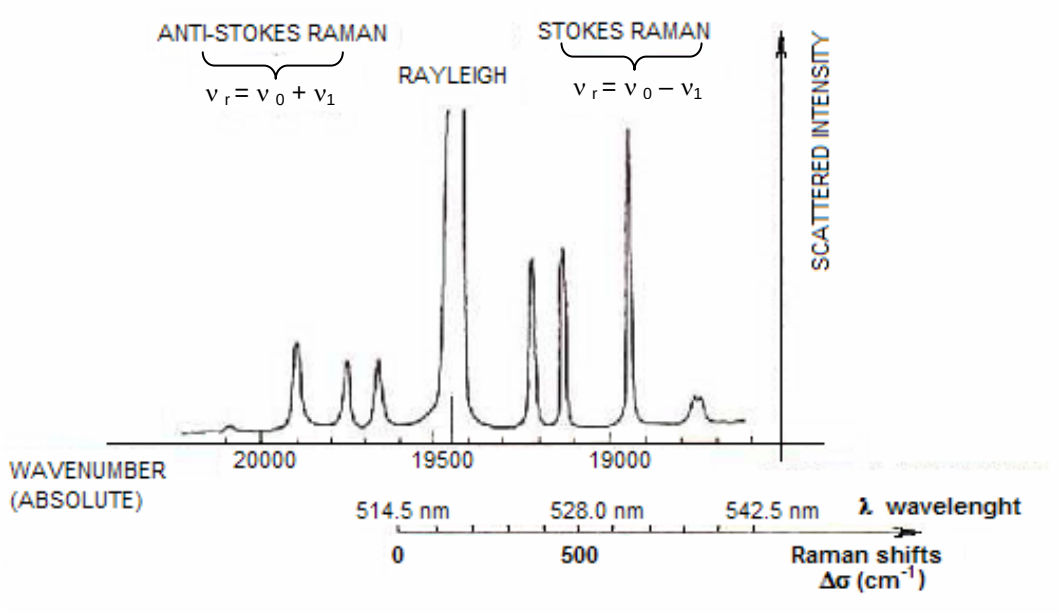

Fig.4.9 *Anti-Stokes and Stokes bands.*

This phenomenon was predicted by Adolf Gustav Smekal (1895-1959) in 1923, theoretically described by Kramers and Heisenberg (1925), Schrödinger (1926), Dirac (1927) and for the first time experimentally identified by the Indian physicist, Chandrasekhara Venkata Raman (1888-1970) in 1928. G.S. Landsberg (1890-1957) and L.I. Mandelstam (1879-1944) found this effect independently and almost simultaneous in Moscow. This effect has also been called the Smekal-Raman effect. If the polarizability of a molecule changes as it rotates or vibrates, incident radiation of frequency ν_0, according to classical theory, should produce scattered radiation, the most intense part of which has unchanged frequency. Recently, two studies have shown that Raman spectroscopy can be applicable for routine analysis of the water content in silicate glasses (Thomas 2000; Chabiron et al. 2004). This method has the advantage of allowing analyses of small (down to 5 μm) and unexposed melt inclusions, of a broad availability and a short analytical time. The area of the water band in the Raman spectra is normalized to the area of the wide band centred at 480 cm^{-1}, which is assigned to asymmetric stretching vibration of T–O–T linkages (Fig. 4.10).

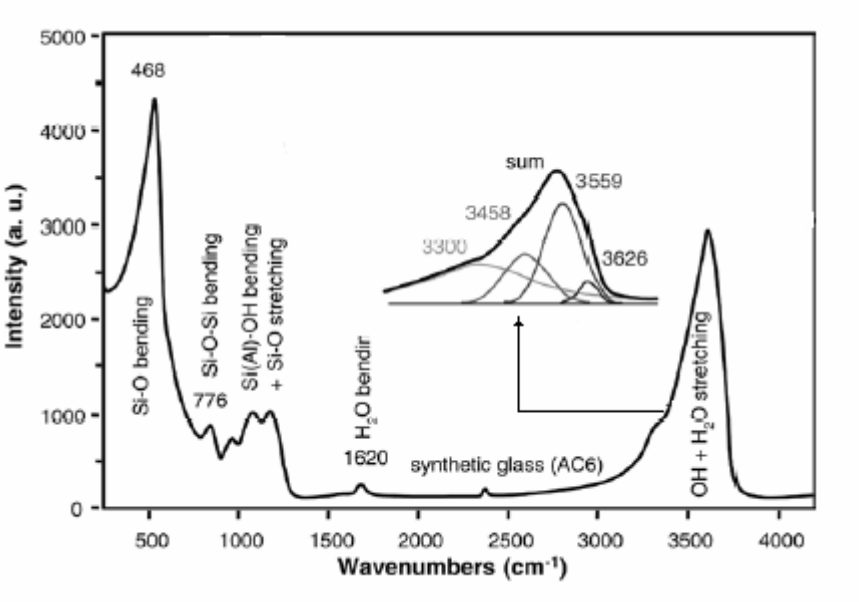

Fig.4.10 *Raman Spectra for water rich inclusion. We can notice the water peak at around 3560 cm^{-1} (Chabiron et al., 2004).*

Thomas et al., 2006 describe a good linear correlation between the normalized area of the water peak and the total water content of their samples.:

$$A_{standard} : A_{sample} = H_2O_{standard} : H_2O_{sample}$$

Total water concentration (H_2O_T) is measured using a JY Horiba LabRam HR800 Visible Raman with a SensIR FTIR system equipped with a Andor electronically cooled CCD detection system (1024x256), a LaserPhysics Reliant 100S-514nm argon laser (adjustable to 100mW maximum), a 25mW-633nm He-Ne laser and an Olympus optical microscope, with a long working distance 80× objective (required for imaging deep inclusions). For all measurements a confocal pinhole of 150 μm was used (see Thomas 2002). All spectra were measured in the high-frequency range between 2800 and 3900 cm^{-1}. For simplicity we have adopted a linear background correction in the integration limits between 3100 and 3750 cm^{-1}.

Cap. 5

SAMPLES

The deposits of Campi Flegrei eruptions have been selected based on age, eruptive characteristic, mineralogical and chemical compositions, structural position of eruptive centre to verify the existence of possible change of the feeding system among several eruptions. The study of the products of eruptions occurred before and after the Neapolitan Yellow Tuff event, can help to understand if eruptions with great magnitude values and characterized by caldera collapse could vary the chemical- physical conditions of a magmatic feeding system. The study of the products of eruptions occurred in the 3 epochs subsequent to the Neapolitan Yellow Tuff event, are helpful to verify the possible stability (regarding composition, residence depth, magma temperature) of a magmatic feeding system in the last period of volcanic activity. From the study of products of different chemical and mineralogical composition, such as those characterized by a different eruptive mechanism, we can learn if difference in chemical-physical conditions of the feeding system of a single eruption exist and if it is possible to outline the chemical and thermal evolution of magma during its rising. The study of the deposits, produced from centres located in different structural settings, may allow to understand if differences exist in chemical-physical conditions of the feeding system of volcanoes that develop along the rim or the centre of caldera.

5.1 SENGA (o FOSSA LUPARA)

Senga eruption occurred in the Third Epoch, about 3.8 ka ago and it is dated with the C^{14} method. It was an explosive hydromagmatic and magmatic eruption occurred at the centre of the Flegrei caldera.

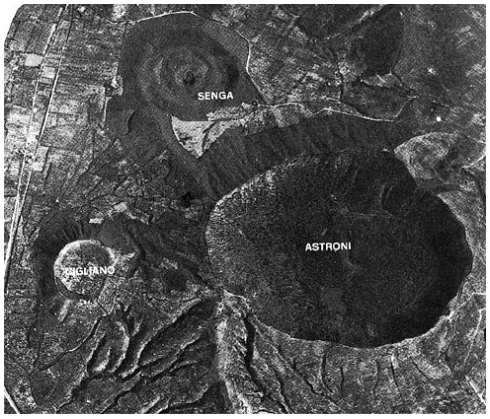

Fig. 5.1 *Location of the sample "Senga".*

Deposits from this site are on cineritic levels, for the most part in the bottom of stratigraphic succession, formed by pumices and scoriae, with lava litic fragments; they lay on Astroni and Solfatara deposits.

5.2 SOLFATARA

Solfatara eruption occurred during the Third Epoch, between 4.1 and 3.8 ka. It was explosive hydromagmatic and magmatic and was located at the centre of the Flegrei caldera. Deposits are on cineritic cohesive levels with pumices, scoriae, and lava litic tuff fragments that are hydrothermalized. Deposits are strongly altered and lay on Monte Olibano and Accademia deposits underling the Astroni deposits.

Fig. 5.2 *Location of the sample "Solfatara".*

5.3 ACCADEMIA

Accademia eruption was an effusive eruption occurred to the East of Starza terrace, with the formation of a dome. Sampled deposits are breccias and lavas, of trachytic and porphyric composition, with the presence of feldspar, pyroxene and biotite crystals. These deposits lay on top of the Agnano Monte Spina and Solfatara deposits. The eruption occurred in the Third Epoch, between 4.1 and 3.8 ka.

Fig. 5.3 *Location of the sample "Accademia".*

5.4 FONDO RICCIO

Fondo Riccio eruption was a very explosive eruption of strombolian type occurred from an eruptive center sited on the western side of Gauro volcano, at the center of the Flegrei caldera. The deposits are a succession of levels with chaotic texture of scoriae and cineritic and sandy levels; they are scoriae (black, of angular shape and at different vesciculation grade) and one bomb. It is present a compositional variation between the basal scoriae and those at the top of the succession. The eruption occurred between 10.3 and 9.5 ka, during the First Epoch.

Fig. 5.4 *Location of the sample "Fondo Riccio".*

5.5 MINOPOLI 2

Minopoli 2 eruption was a strombolian eruption with hydromagmatic phases occurred at an eruptive center sited in the Northern side of the caldera. Deposits are scoriae and ash levels lying on top of the Soccavo 1 deposits. Scoriae are grey-black with trachybasaltic, alkali-trachytic and porphyric composition, with the presence of olivine pyroxene and biotite crystals. The eruption occurred between 10.3 and 9.5 ka, during the First Epoch.

Fig. 5.5 *Location of the sample "Minopoli 2".*

5.6 MINOPOLI 1

Minopoli 1 eruption was an explosive strombolian eruption with hydromagmatic phases occurred at an eruptive center sited in the Northern side of the caldera. Deposits are constituted by scoriae and ash levels, lay on Mean Pumices deposits and underlay the Montagna Spaccata deposits. Scoriae are grey-black with trachybasaltic, alkali-trachytic and porphyric composition for presence of olivine pyroxene and biotite crystals. The eruption occurred between 11.1 and 10.3 ka, during the First Epoch.

Fig. 5.6 *Location of the sample "Minopoli 1".*

5.7 CAPO MISENO

Capo Miseno eruption was an explosive hydromagmatic eruption occurred by an eruptive centre sited on the western side of caldera. The deposits, consisting in tuff, pumices, scoriae and few litics, lay on Porto Miseno deposits and underlay the "A" paleosoil. Grey scoriae are well vesciculated with trachytic and porphyric composition for the presence of feldspar, pyroxene and biotite. The eruption occurred between 14-12 and 8.6 ka, during the First Epoch.

Fig. 5.7 *Location of the sample "Capo Miseno".*

5.8 PORTO MISENO

Porto Miseno eruption was an explosive hydromagmatic eruption and latterly magmatic occurred from a centre sited on the eastern side of the caldera. The deposit is well hardened tuff with ash on pumices and lithics; in the upper part it is present a fall level with pumices and lavas lithic; the pumices in the tuff are distributed discontinuously. The deposits lay on Bacoli and Capo Miseno deposits and are grey, well vesciculated, trachytic and porphyric pumices, with pyroxene, feldspar and biotite crystals. The eruption occurred between 14-12 and 8.6 ka, during the First Epoch.

Fig. 5.8 *Location of the sample "Porto Miseno".*

5.9 TORREGAVETA

Torregaveta eruption was an explosive eruption of subplinian type occurred in the South-Western side of the caldera. The deposits are constituted by two scoria levels with altered material fragments and lava blocks and an intermediate ash-sandy level. These deposits lay on Breccia Museo and underlay to Solchiaro and the Neapolitan Yellow Tuff. Scoriae are dark beige, angular and vesciculated, with latitic and porphyric composition for the presence of pyroxene, biotite and feldspar. The eruption occurred between 39-37 and 17.2 ka.

Fig. 5.9 *Location of the sample "Torregaveta".*

Cap. 6

DATA AND RESULTS

Products from two eruptions that occurred in the First Epoch were studied. The Fondo Riccio eruption occurred at 9.5 ka from an eruptive center on the western side of the Gauro volcano, near the center of the Phlegraean caldera. The eruption was explosive, with strombolian character. The eruptive deposits are composed of coarse scoria beds with subordinate coarse-ash beds and overlay Montagna Spaccata tephra and are in turn overlain by paleosol A (Di Vito et al., 1999). The Minopoli 1 eruption was a magmatic eruption, with hydromagmatic phases, that occurred at 11.1 ka, along a regional fault system in the northern sector of the Phlegraean caldera. The eruptive products are composed of alternating pumice lapilli fallout and mainly massive ash fallout, and less abundant cross laminated ash surge beds. The deposits overlay Pomici Principali and are overlain by Montagna Spaccata (Di Vito et al., 1999).

Sample CF-FR-C1 is a scoria and sample CF-FR-C2 is a lava bomb from the Fondo Riccio unit. Both samples are porphyritic latite, with abundant crystals in a glassy, vesicular groundmass, and were deposited between 9.5 and 10.3 ka (Di Vito et al., 1999). The bulk rock contains less than 10% phenocrysts, which include clinopyroxene, olivine and biotite with subordinate plagioclase and magnetite. In thin section clinopyroxene and plagioclase are found in small clots; these minerals also occur among microlites. Silicate MI in olivine and pyroxene phenocrysts from sample FR-C1 and in clinopyroxenes for the sample FR-C2 were studied. For the Minopoli 1 unit, sample MI1-C1 is a scoria and sample

MI1-C2 is a cohesive scoria sampled along the caldera rim, and was likely erupted during the final magmatic stage of the eruption. The deposits include scoria and ash layers. Both samples are porphyritic trachybasalt and range from 11.1 and 10.3 ka (Di Vito et al, 1999). The bulk rock contains about 20% phenocrysts, which include clinopyroxene, olivine and biotite. Silicate MI in olivine and pyroxene from Mi1-C1 and in clinopyroxene from MI1-C2 were studied.

The abundance of MI varies from crystal to crystal in the same sample. Melt inclusions consist of silicate glass, generally devitrified, with a shrinkage bubble and daughter crystals (usually apatite or Fe/Ti oxides). MI generally have elongated rectangular shapes and range from 30 to 80 μm (most between 20 and 50 μm) (Fig. 6.1). Rock samples were hand crushed and phenocrysts were hand picked, mounted on a glass slide, and doubly polished to improve the optical clarity during microscope heating experiments.

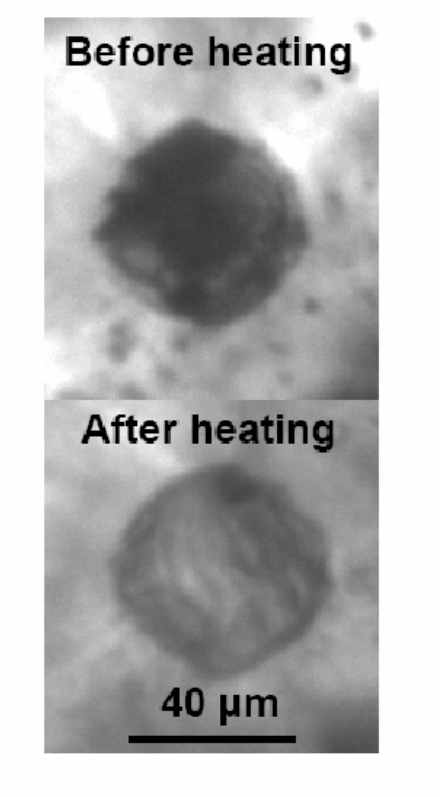

Fig. 6.1 *Change in appearance of a silicate melt inclusions hosted in clinopyroxene in Fondo Riccio scoria as a result of heating from room temperature (22ºC) to the homogenization temperature (1137ºC). After heating to 1137ºC the inclusion contains only a vapour bubble. The MI is approximately 40 μm in diameter.*

Fondo Riccio olivine compositions range from Fo_{84} to Fo_{87}, while Minopoli 1 olivines range from Fo_{77} to Fo_{78} (Fig. 6.2). Clinopyroxene compositions fall in the diopside-salite field (Wo_{44-48}, Fs_{5-19}) and Mg # (calculated based on total Fe) varies from about 73.4 to 88.6 for Fondo Riccio samples (with a compositional gap between 78 and 83) and from about 85.1 to 89.9 for Minopoli 1 samples. Clinopyroxenes are low-Ti, which is a characteristic of "HKS"- type lavas of the Roman Comagmatic Province (Cundari and Fergusson, 1982).

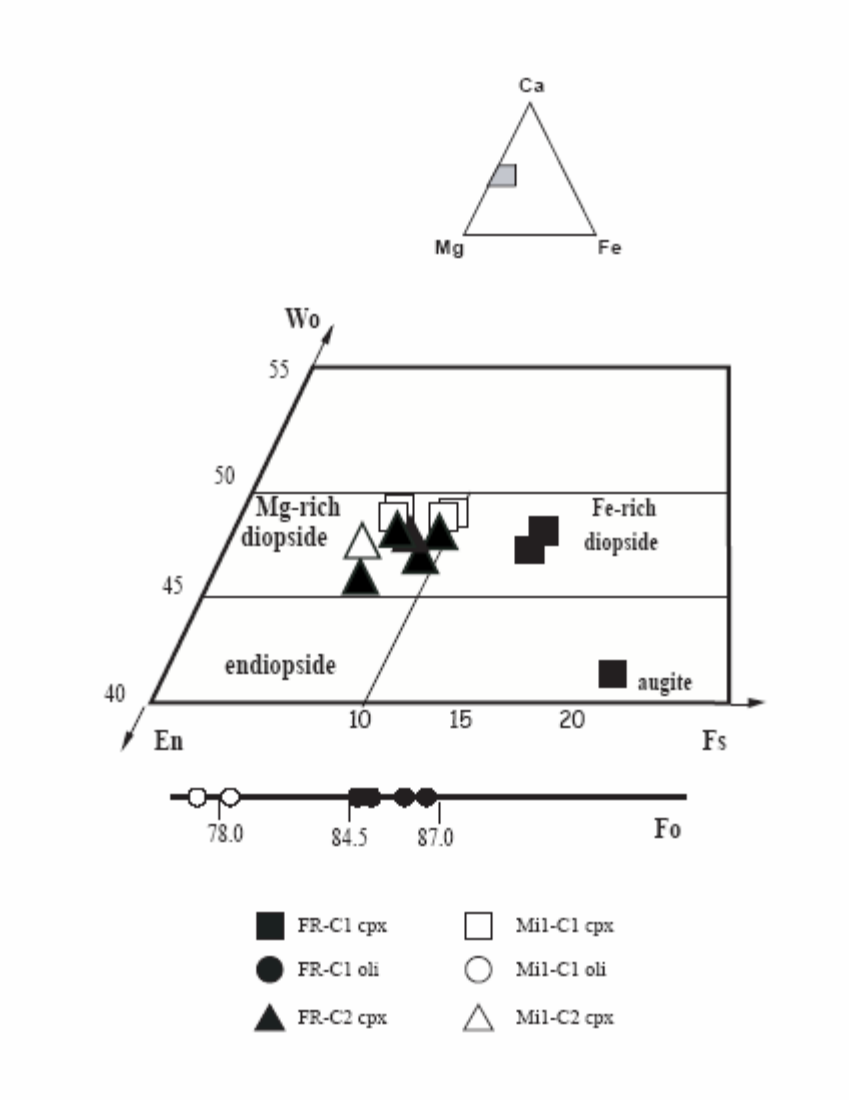

Fig. 6.2 *Classification diagrams for pyroxene and olivine phenocrysts (Morimoto, 1988). Filled squares = compositions of MI hosted in clinopyroxene from FR-C1 (scoria); filled circles = composition of MI hosted in olivine from FR-C1 (scoria); filled triangles = compositions of MI hosted in clinopyroxene from FR-C2 (bomb); open squares = compositions of MI hosted in clinopyroxene from Mi1-C1; open circles = compositions of MI hosted in olivine from Mi1-C1; open triangles = composition of MI hosted in clinopyroxenes from Mi1-C2.*

Homogenization temperatures of MI in clinopyroxene and olivine from the scoria of Fondo Riccio (FR-C1) average 1135 ± 3°C and 1155 ± 3°C, respectively, whereas MI in clinopyroxene from the bomb sample (FR-C2) average 1159 ± 3 °C. Homogenization temperatures of Minopoli 1 MI in clinopyroxenes average 1132 ± 3°C and those in olivine average 1145 ± 3°C.

The maximum temperature achieved during heating experiments does not equal the trapping temperature because a bubble still remained in the inclusions. MI compositions can be depleted in the host mineral components if the maximum temperature of heating is below the trapping temperature. Thus, the concentrations of most elements in the quenched MI may not reflect their original values in the trapped melt. However, ratios of elements that are incompatible in the host, and also concentrations of elements that are present at similar levels in the melt and the host, should not be significantly affected by over- or under-heating. Moreover, Fedele et al. (2003) have shown that compositions of MI obtained from inclusions that were heated until all of the solids had melted (with the bubble still present) and quenched were in good agreement with melt compositions predicted by the MELTS program (see also Thomas et al, 2002).

Representative compositions of MI (average values) hosted in Fondo Riccio clinopyroxene and olivine are shown together with MI size, maximum temperature (T_{run}) and host crystal Mg# in Table 6.1 (FR-C1) and Table 6.2 (FR-C2). Representative compositions of MI from Minopoli 1 are shown in Table 6.3. All MI are characterized by analytical totals < 100. This is interpreted to reflect the presence of H_2O in the MI, as confirmed by secondary ion mass spectrometry (SIMS) analyses that show average H_2O contents between 3.3 - 6.9 wt% for Fondo Riccio samples and between 1.3-5.2 wt % for Minopoli 1 samples (Tables 6.1-6.3).

MI from Fondo Riccio show a broad range for SiO_2 (46.8 - 59.3 wt%), CaO (3.66 - 12.4 wt%), Na_2O (1.3-3.7 wt%) and K_2O+Na_2O (4.19 - 9.73 wt%). Conversely, MI from Minopoli 1 show narrow ranges for SiO_2 (49.6 -51.8 wt%), CaO (7.6 – 13.3 wt%), Na_2O (1.0-1.8 wt%) and K_2O+Na_2O (4.19 - 9.73 wt%) as shown in Tables 6.1-6.3.

Sample	FR-C1	FR-C1	FR-C1	FR-C1	FR-C1	FR-C1	FR-C1	FR-C1	FR-C1	FR-C1	FR-C1	FR-C1	FR-C1	FR-C1	FR-C1
MI label	p6 M1	p6 M2	p6 M4	p6 M5	p6 M6	p6 M7	p6 M8	p6 M9	p11 M1	p12 M1	p12 M2	o1 M1	o2 M1	o4 M1	o6 M1
Size (µm)	75	80	35	30	60	55	75	55	85	50	130	70	50	60	50
Host xl	cpx	cpx	cpx	cpx	cpx	cpx	cpx	cpx	cpx	cpx	cpx	ol	ol	ol	ol
T (quen)°C	1126	1126	1126	1126	1126	1126	1126	1126	1145	1139	1139	1172	1150	1175	1135
Host Mg#	74.41	73.37	73.68	75.16	76.11	83.17	78.04	86.12	83.17	78.04	86.12	86.77	86.56	84.95	84.70
Host xl composition															
SiO_2	49.93	50.24	50.24	50.36	50.36	50.36	50.74	50.41	51.68	49.01	49.80	40.15	40.02	40.74	39.77
TiO_2	0.62	0.63	0.63	0.63	0.63	0.63	0.59	0.53	0.32	0.77	0.67	0.05	0.00	0.04	0.00
Al_2O_3	3.21	3.35	3.35	3.02	3.02	3.02	3.27	3.17	3.02	4.13	3.63	0.01	0.01	0.03	0.02
FeO	8.52	8.71	8.71	8.71	8.71	8.71	8.17	7.99	5.62	7.43	6.49	13.06	12.90	13.89	14.71
MnO	0.44	0.48	0.48	0.40	0.40	0.40	0.39	0.39	0.11	0.24	0.21	0.23	0.25	0.28	0.30
MgO	13.90	13.47	13.47	13.68	13.68	13.68	13.87	14.27	15.59	14.83	15.23	48.06	46.62	44.00	45.71
CaO	22.45	22.41	22.41	22.25	22.25	22.25	22.04	21.92	22.78	21.91	22.37	0.36	0.32	0.30	0.31
Na_2O	0.36	0.41	0.41	0.37	0.37	0.37	0.34	0.37	0.17	0.28	0.22	0.03	0.01	0.01	0.01
K_2O	0.02	0.00	0.00	0.02	0.02	0.02	0.01	0.00	0.01	0.01	0.02	0.02	0.01	0.00	0.03
P_2O_6	0.02	0.02	0.02	0.02	0.02	0.02	0.03	0.00	0.01	0.01	0.01	0.02	0.01	0.00	0.02
Total	99.57	99.99	99.99	99.67	99.67	99.67	99.50	99.09	99.36	98.71	98.70	102.14	98.82	99.38	100.90
Wo	27.3	27.3	27.3	27.3	27.3	27.3	27.3	27.3	51.7	50.5	50.5	0.6	0.5	0.5	0.5
En	56.5	56.5	56.5	56.5	56.5	56.5	56.5	56.5	35.4	34.4	34.4	77.9	77.6	75.3	74.9
Fs	16.2	16.2	16.2	16.2	16.2	16.2	16.2	16.2	13.0	15.1	15.1	21.5	21.9	24.2	24.6
Melt inclusions composition															
Electron Microprobe															
SiO_2	57.86	58.12	58.18	58.80	58.16	58.30	59.38	56.06	52.06	55.06	48.33	47.69	46.83	48.09	49.57
TiO_2	0.53	0.54	0.48	0.51	0.53	0.46	0.47	0.61	0.72	0.66	0.98	0.87	0.89	0.94	0.87
Al_2O_3	16.32	16.61	17.55	16.35	17.33	16.56	18.32	17.44	18.88	18.19	14.39	13.88	12.77	14.31	16.52
FeO^{tot}	4.01	3.58	2.77	3.54	2.97	3.61	1.98	5.21	4.68	3.51	5.94	7.21	8.22	7.71	6.86
MnO	0.26	0.23	0.16	0.32	0.14	0.16	0.13	0.07	0.15	0.06	0.11	0.12	0.18	0.17	0.18
MgO	1.91	1.74	1.44	1.64	1.47	1.66	1.21	2.05	3.08	2.25	6.11	8.05	9.45	6.92	4.91
CaO	4.81	4.74	4.14	4.54	4.16	4.51	3.66	5.02	7.32	7.42	11.35	10.15	9.42	9.96	9.86
Na_2O	3.40	3.61	3.60	3.38	3.73	3.53	3.57	3.60	3.70	2.54	1.73	1.57	1.33	1.41	1.72
K_2O	7.65	7.78	8.18	7.69	8.25	7.94	8.57	7.12	5.42	6.92	4.64	4.67	4.41	4.58	5.21
P_2O_6	0.22	0.14	0.27	0.14	0.21	0.14	0.27	0.30	1.03	0.31	0.87	0.61	0.62	0.56	0.67
NiO	0.00	0.00	0.00	0.00	0.00	0.00	0.00	0.00	0.00	0.00	0.00	0.00	0.00	0.00	0.00
SO_2	0.07	0.06	0.04	0.13	0.08	0.07	0.09	0.04	0.16	0.05	0.29	0.33	0.40	0.31	0.25
F	0.21	0.12	0.14	0.17	0.17	0.22	0.28	0.17	0.31	0.00	0.08	0.27	0.14	0.15	0.18
Cl	0.58	0.71	0.57	0.56	0.54	0.62	0.53	0.46	0.58	0.32	0.47	0.42	0.44	0.47	0.42
Total	97.83	97.96	97.52	97.76	97.74	97.76	98.46	98.15	98.09	97.27	95.29	95.85	95.08	95.58	97.22
Ion Microprobe															
H_2O (wt%)	-	6.96	-	-	-	-	3.66	-	-	-	-	4.13	-	3.61	-
Li ppm	-	28	-	-	-	-	26	-	-	-	-	15	-	11	-
Be	-	13	-	-	-	-	16	-	-	-	-	9	-	52	-
B	-	62	-	-	-	-	59	-	-	-	-	39	-	55	-
Rb	-	316	-	-	-	-	316	-	-	-	-	218	-	276	-
Sr	-	627	-	-	-	-	614	-	-	-	-	1043	-	902	-
Y	-	53	-	-	-	-	35	-	-	-	-	45	-	43	-
Zr	-	384	-	-	-	-	262	-	-	-	-	176	-	292	-
Nb	-	49	-	-	-	-	48	-	-	-	-	23	-	35	-
Cs	-	25	-	-	-	-	16	-	-	-	-	19	-	19	-
Ce	-	172	-	-	-	-	128	-	-	-	-	112	-	98	-
Nd	-	47	-	-	-	-	32	-	-	-	-	38	-	97	-
Sm	-	1	-	-	-	-	1	-	-	-	-	2	-	3	-
Dy	-	4	-	-	-	-	<1	-	-	-	-	2	-	3	-
Yb	-	1	-	-	-	-	<1	-	-	-	-	2	-	2	-
Th	-	29	-	-	-	-	25	-	-	-	-	21	-	19	-
U	-	12	-	-	-	-	7	-	-	-	-	5	-	9	-

Table 6.1 *Fondo Riccio C1 . MI composition determined by EMPA and SIMS. *T(run) = maximum temperature of heating experiment. Cpx = clinopyroxene host crystal. Ol = olivine host crystal.*

Sample	FR-C2	FR-C2	FR-C2	FR-C2	FR-C2
MI label	p2 M1	p4 M1	p5 M1	p6 M1	p7 M1
Size (µm)	20	40	80	100	40
Host xl	cpx	cpx	cpx	cpx	cpx
T (quen)°C	1176	1135	1165	1152	1164
Host Mg#	88.68	86.94	88.57	84.98	84.62
Host xl composition					
SiO_2	53.70	52.03	52.11	51.25	51.67
TiO_2	0.36	0.44	0.39	0.60	0.54
Al_2O_3	2.09	2.48	2.11	2.79	3.21
FeO	3.76	4.38	3.93	5.06	5.00
MnO	0.10	0.14	0.08	0.17	0.12
MgO	16.53	16.36	17.09	16.07	15.44
CaO	23.25	23.01	23.00	22.47	23.02
Na_2O	0.11	0.11	0.09	0.15	0.12
K_2O	0.00	0.01	0.02	0.01	0.00
P_2O_6	0.02	0.04	0.01	0.06	0.01
Total	100.07	99.05	98.94	98.67	99.20
Wo	53.3	52.4	52.2	51.3	52.8
En	37.9	37.3	38.8	36.7	35.4
Fs	8.8	10.3	9.1	11.9	11.7
Melt inclusions composition					
Electron Microprobe					
SiO_2	49.09	49.08	48.87	47.72	53.01
TiO_2	1.00	0.97	0.91	1.28	1.06
Al_2O_3	12.84	13.86	12.76	12.81	20.34
FeO^{tot}	7.00	5.94	6.57	7.92	3.44
MnO	0.10	0.15	0.15	0.28	0.16
MgO	6.81	6.17	7.33	6.90	2.12
CaO	10.65	11.27	11.88	12.40	6.06
Na_2O	1.31	1.42	1.46	1.36	2.83
K_2O	4.07	4.20	4.23	2.60	7.83
P_2O_6	0.60	0.36	0.44	0.46	1.36
NiO	0.00	0.00	0.00	0.00	0.00
SO_2	0.34	0.27	0.19	0.26	0.13
F	0.07	0.40	0.18	0.10	0.08
Cl	0.44	0.40	0.43	0.33	0.39
Total	94.31	94.49	95.40	94.42	98.81
Ion Microprobe					
H_2O	3.25	-	-	-	-
Li	11	-	-	-	-
Be	3	-	-	-	-
B	24	-	-	-	-
Rb	98	-	-	-	-
Sr	431	-	-	-	-
Y	25	-	-	-	-
Zr	136	-	-	-	-
Nb	16	-	-	-	-
Cs	15	-	-	-	-
Ce	48	-	-	-	-
Nd	16	-	-	-	-
Sm	3	-	-	-	-
Dy	1	-	-	-	-
Yb	1	-	-	-	-
Th	7	-	-	-	-
U	6	-	-	-	-

Table 6.2 *Fondo Riccio C2 . MI composition determined by EMPA and SIMS. *T(run) = maximum temperature of heating experiment. Cpx = clinopyroxene host crystal. Ol = olivine host crystal.*

Sample	Mi 1-C1	Mi 1-C1	Mi 1-C1	Mi 1-C1	Mi 1-C1	Mi 1-C1	Mi 1-C1	Mi 1-C2	Mi 1-C2
MI label	p2 M1	p3 M1	p6 M1	p6 M2	p8 M1	o5 M1	o6 M1	p1 M1	p1 M2
Size (µm)	50	60	50	70	40	60	55	45	50
Host xl	cpx	cpx	cpx	cpx	cpx	olivine	olivine	cpx	cpx
T (quen)°C	1122	1149	1156	1156	1108	1120	1145	1122	1122
Host Mg#	86.64	88.59	85.10	86.10	86.29	86.68	85.68	89.89	89.89
Host xl composition									
SiO_2	52.39	52.96	52.52	52.52	52.78	39.38	38.96	52.67	52.67
TiO_2	0.41	0.33	0.43	0.43	0.36	0.00	0.01	0.25	0.25
Al_2O_3	3.03	2.19	3.35	3.35	2.78	0.02	0.02	1.68	1.68
FeO	4.36	3.72	4.97	4.97	4.58	12.66	13.70	3.37	3.37
MnO	0.14	0.10	0.10	0.10	0.11	0.20	0.22	0.09	0.09
MgO	15.86	16.20	15.92	15.92	16.18	46.22	45.99	16.82	16.82
CaO	22.75	23.39	21.52	21.52	22.53	0.28	0.27	23.53	23.53
Na_2O	0.14	0.13	0.15	0.15	0.13	0.02	0.04	0.15	0.15
K_2O	0.01	0.03	0.02	0.02	0.01	0.03	0.01	0.01	0.01
P_2O_5	0.02	0.04	0.00	0.00	0.00	0.00	0.02	0.00	0.00
Total	99.11	99.07	98.99	98.99	99.45	98.82	99.22	98.56	98.56
Wo	52.8	53.9	50.6	50.6	51.9	0.5	0.4	53.7	53.7
En	36.8	37.3	37.5	37.5	37.3	77.9	76.4	38.4	38.4
Fs	10.4	8.8	11.9	11.9	10.8	21.7	23.1	7.9	7.9
Melt inclusions composition									
Electron Microprobe									
SiO_2	46.94	48.20	51.79	49.96	50.19	47.81	47.96	51.11	50.75
TiO_2	1.05	0.76	0.68	0.76	0.79	0.66	0.78	0.72	0.90
Al_2O_3	13.97	11.98	10.70	10.15	16.54	13.81	14.61	13.18	13.47
FeO^{tot}	9.58	8.20	7.50	7.66	5.99	6.80	7.73	6.84	7.11
MnO	0.29	0.10	0.21	0.15	0.17	0.12	0.08	0.10	0.17
MgO	5.65	8.00	7.98	8.93	5.40	11.53	9.37	6.92	6.93
CaO	10.80	12.75	12.23	13.35	9.20	7.57	8.94	10.34	11.01
Na_2O	1.82	1.30	1.16	1.03	1.71	1.50	1.57	1.24	1.30
K_2O	3.24	3.17	2.91	2.58	4.76	4.11	3.92	3.88	4.07
P_2O_5	0.38	0.38	0.26	0.24	0.70	0.98	0.56	0.64	0.62
NiO	0.14	0.05	0.04	0.00	0.02	0.08	0.05	0.00	0.00
SO_2	0.11	0.91	0.09	0.10	0.10	0.34	0.21	0.31	0.37
F	0.29	0.03	0.01	0.03	0.09	0.07	0.17	0.00	0.00
Cl	0.30	0.28	0.20	0.20	0.34	0.43	0.43	0.42	0.39
Total	94.56	96.11	95.74	95.14	96.00	95.81	96.38	95.68	97.06
Ion Microprobe									
H_2O	5.15	-	1.93	1.29	5.28	3.89	4.40	5.15	-
Li	21	-	11	12	24	7	18	21	-
Be	14	-	7	77	7	12	1	14	-
B	31	-	27	320	44	36	32	47	-
Rb	97	-	324	122	215	168	167	176	-
Sr	667	-	614	480	765	607	889	646	-
Y	92	-	52	63	37	27	42	37	-
Zr	266	-	262	160	162	437	116	139	-
Nb	14	-	48	14	23	19	16	22	-
Cs	6	-	16	4	16	10	8	93	-
Ce	180	-	128	83	88	69	87	79	-
Nd	180	-	32	74	63	61	75	53	-
Sm	4	-	1	2	2	1	1	1	-
Dy	2	-	<1	1	1	<1	<1	<1	-
Yb	<1	-	1	<1	1	<1	<1	<1	-
Th	5	-	25	3	14	9	6	13	-
U	1	-	7	2	4	3	<1	<1	-

Table 6.3 *Minopoli 1 C1 and C2 . MI composition determined by EMPA and SIMS. *T(run) = maximum temperature of heating experiment. Cpx = clinopyroxene host crystal. Ol = olivine host crystal.*

On the total alkali-SiO_2 classification diagram (Fig.6.3; Le Bas et al., 1986) the Fondo Riccio bulk-rock composition is in the latite field. Fondo Riccio MI data show two trends: from latite to trachyte for MI in Fe-rich diopside (sample CF-FR-C1) and from trachybasalt to shoshonite for MI in both Mg-rich diopside (sample CF-FR-C2) and olivine (sample CF-FR-C1). The Minopoli 1 bulk-rock composition is in the trachyandesite field, whereas MI data show two different compositions: basalt for MI in clinopyroxenes from the lower unit (Mi1-C1) and trachybasalt for MI in olivine (Mi1-C1) and clinopyroxenes from the upper unit (Mi1-C2). Except for clinopyroxene in FR-C1, MI are generally less evolved than the corresponding host rock. In particular, MI in olivine from CF-FR-C1 scoria show the same, less evolved composition as MI in clinopyroxene from CF-FR-C2 bomb sample.

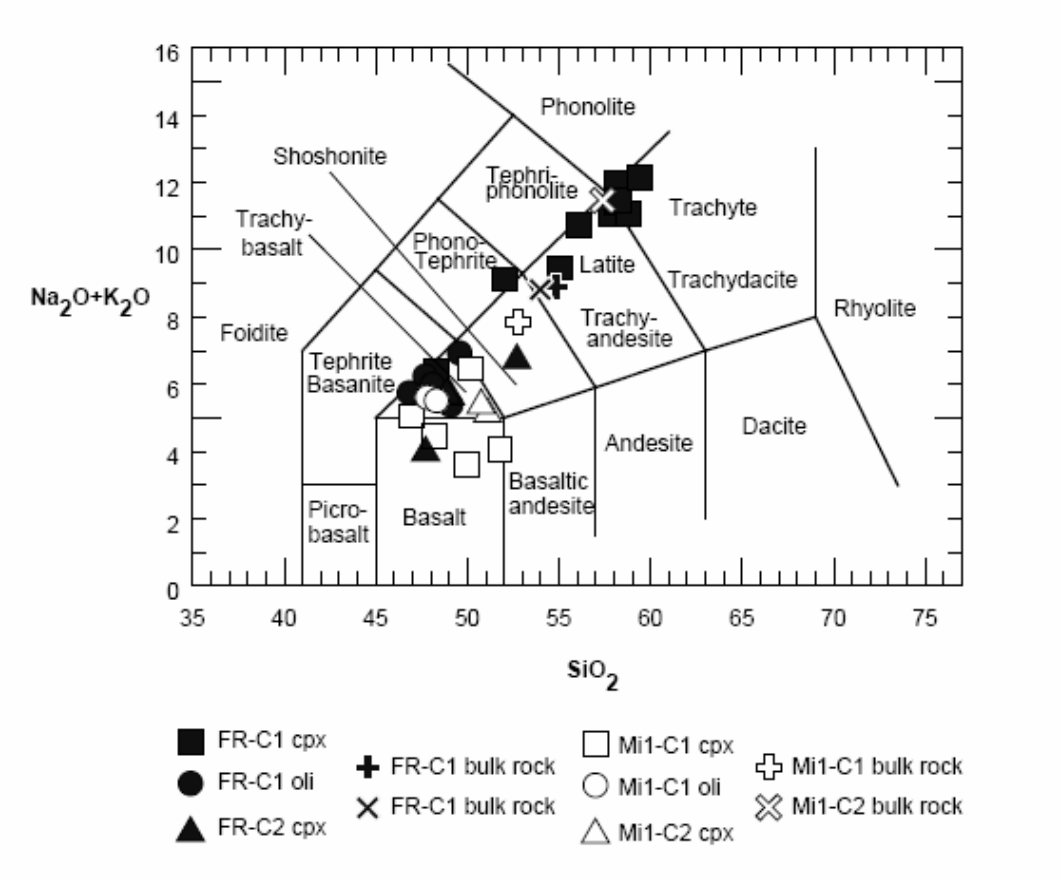

Fig. 6.3 *Total alkali-silica diagram (Le Bas et al., 1986) showing compositions of MI hosted in clinopyroxene and olivine from Fondo Riccio and Minopoli 1. Bulk rock compositions are also shown.*

The Fondo Riccio bulk rock is depleted in K_2O (not shown in the variation diagrams) and enriched in TiO_2 and Na_2O compared with MI with similar Mg# hosted in clinopyroxene from the CF-FR-C1 scoria sample. Harker diagrams showing major element concentrations of MI as a function of SiO_2 show a wider range in composition in Fondo Riccio samples than Minopoli 1 (Fig. 6.4). MI in clinopyroxene and olivine from both samples show decreasing Al_2O_3 (Fig. 6.4a) and Na_2O (Fig. 6.4f) and increasing FeO^{tot} (Fig. 6.4b), TiO_2 (Fig. 6.4c), MgO (Fig. 6.4d) and CaO (Fig. 6.4e) with decreasing SiO_2. These trends are consistent with crystallization of olivine and clinopyroxene from alkali basalt magma. In particular, the trends described above suggest earlier crystallization of olivine in the CF-FR-C1 sample and clinopyroxene in the CF-FR-C2 sample compared with the timing of crystallization of clinopyroxene in the CF-FR-C1 scoria sample. The TiO_2 contents of these MI are consistent with the low Ti-contents of lavas from the Roman Comagmatic Province. To explain Ti enrichment in the bulk rock compared with MI (whose compositions should represent the melt composition before the eruption), the studied rocks would have to contain about 60% groundmass and ≈ 40% phenocrysts (clinopyroxene, olivine, feldspar and biotite), which is a higher phenocryst abundant than that observed in thin sections. If we assume that the groundmass has a composition similar to MI in more evolved clinopyroxene, then TiO_2 bulk-rock contents are compatible with analyzed values (Table 6.1-6.3and Table 6.4).

It is more difficult to explain Na_2O enrichment in the bulk rock, even though Na_2O in the melt is expected to increase during crystallization (Na behaves as an incompatible element during magma fractionation). We also observe a greater Na enrichment in Fondo Riccio bulk rock compared to Minopoli1 bulk rock. Hydrothermal activity is present in the vicinity of the Fondo Riccio eruption and, as explained for similar behavior at Vesuvius (Lima et al., in press), Na_2O enrichment in the bulk rock most likely represents the effects of hydrothermal fluids. During explosive eruptions associated with decompression during magma ascent, the reaction of NaCl with H_2O at low pressure (< 300 bars) becomes important and hydrolysis reactions produce HCl and NaOH that remain preferentially in the melt (Veksler, 2004). Note that the trend in Na enrichment

observed here is the opposite of that observed during subsolidus hydrothermal alteration of melt inclusions in porphyry copper systems (Student and Bodnar, 2004).

		CF-FR-C1	RE CF-FR-C1	CF-FR-C2	CF-MI1-C1	CF-MI1-C2
SiO_2	wt%	54.76	54.68	54.10	52.76	57.40
Al_2O_3	wt%	17.99	18.11	17.98	17.32	17.97
Fe_2O_3	wt%	7.26	7.23	7.61	7.44	4.87
MgO	wt%	2.33	2.31	2.53	3.53	1.26
CaO	wt%	5.62	5.64	5.97	7.79	3.94
Na_2O	wt%	4.49	4.59	4.46	3.05	3.52
K_2O	wt%	4.35	4.34	4.35	4.79	7.94
TiO_2	wt%	0.82	0.82	0.86	0.87	0.53
P_2O_5	wt%	0.52	0.51	0.58	0.58	0.23
MnO	wt%	0.13	0.13	0.13	0.12	0.12
Cr_2O_3	wt%	0.03	0.03	0.01	0.01	0.02
Ni	ppm	12.00	13.00	6.00	19.00	6.00
Sc	ppm	10.00	10.00	11.00	15.00	5.00
LOI	wt%	1.20	1.10	0.90	1.30	1.80
TOT/C	wt%	0.01	0.01	0.01	0.05	0.03
TOT/S	wt%	0.01	0.01	0.01	0.01	0.05
SUM	wt%	99.50	99.49	99.48	99.56	99.59
FeO*	wt%	3.2	3.2	4.05	4.17	2.39
Mo	ppm	2.40	2.5	2	1.6	0.5
Cu	ppm	7.40	6.6	7.5	15.3	3.8
Pb	ppm	6.50	6.3	7.2	10.8	3.9
Zn	ppm	62.00	60	73	44	9
Ni	ppm	5.30	5	3	7.6	2.9
As	ppm	4.70	4.8	5.7	3.8	1.9
Cd	ppm	<.1	<.1	<.1	0.1	<.1
Sb	ppm	0.20	0.2	0.2	0.1	0.1
Bi	ppm	0.10	0.1	<.1	0.1	0.1
Ag	ppm	<.1	<.1	<.1	<.1	<.1
Au	ppm	1.00	<.5	2.4	1.6	2.5
Hg	ppm	<.01	<.01	0.01	0.01	<.01
Tl	ppm	0.50	0.5	0.2	0.5	0.1
Se	ppm	<.5	<.5	<.5	<.5	<.5
Ba	ppm	1719.20	1654	1712.1	1715.2	1048.9
Be	ppm	7.00	9	7	7	10
Co	ppm	15.90	16.4	17.2	21.5	7.6
Cs	ppm	16.90	16.7	16.2	11.8	16.1
Ga	ppm	20.10	19.6	20.7	19.4	18.1
Hf	ppm	6.40	6.5	6.4	5	6.8
Nb	ppm	35.00	33.5	33.2	26.7	42.1
Rb	ppm	274.80	269.6	309.6	238.5	305.1
Sn	ppm	3.00	2	3	3	4
Sr	ppm	903.00	889.4	919.8	946	724.7
Ta	ppm	1.80	1.8	1.8	1.4	2.3
Th	ppm	22.10	24.2	22.8	18.1	29.7
U	ppm	6.80	6.8	6.1	5.2	9
V	ppm	193.00	190	209	208	110
W	ppm	4.00	4	3.5	4.6	6.5
Zr	ppm	233.20	229.6	229.2	182	267.9
Y	ppm	32.50	31.8	33.4	28.7	32.1
La	ppm	64.10	63.6	63.7	56	74.3
Ce	ppm	123.60	121.7	123.8	109.7	139.6
Pr	ppm	13.40	13.39	13.74	12.37	14.82
Nd	ppm	53.90	53.3	56.8	49.2	57
Sm	ppm	10.10	10	10.5	9.7	9.9
Eu	ppm	2.37	2.28	2.5	2.24	2.27
Gd	ppm	7.66	7.37	7.78	6.99	7.14
Tb	ppm	1.08	1.05	1.1	1.03	1.04
Dy	ppm	5.89	5.85	5.97	5.47	5.65
Ho	ppm	1.08	1.06	1.07	0.99	1.07
Er	ppm	2.89	2.9	2.95	2.68	2.95
Tm	ppm	0.45	0.42	0.44	0.38	0.46
Yb	ppm	2.48	2.6	2.63	2.41	2.65
Lu	ppm	0.41	0.41	0.42	0.36	0.41

* = FeO by dichromate tritation

Table 6.4 *Fondo Riccio and Minopoli 1 bulk rock compositions determined by XRF.*

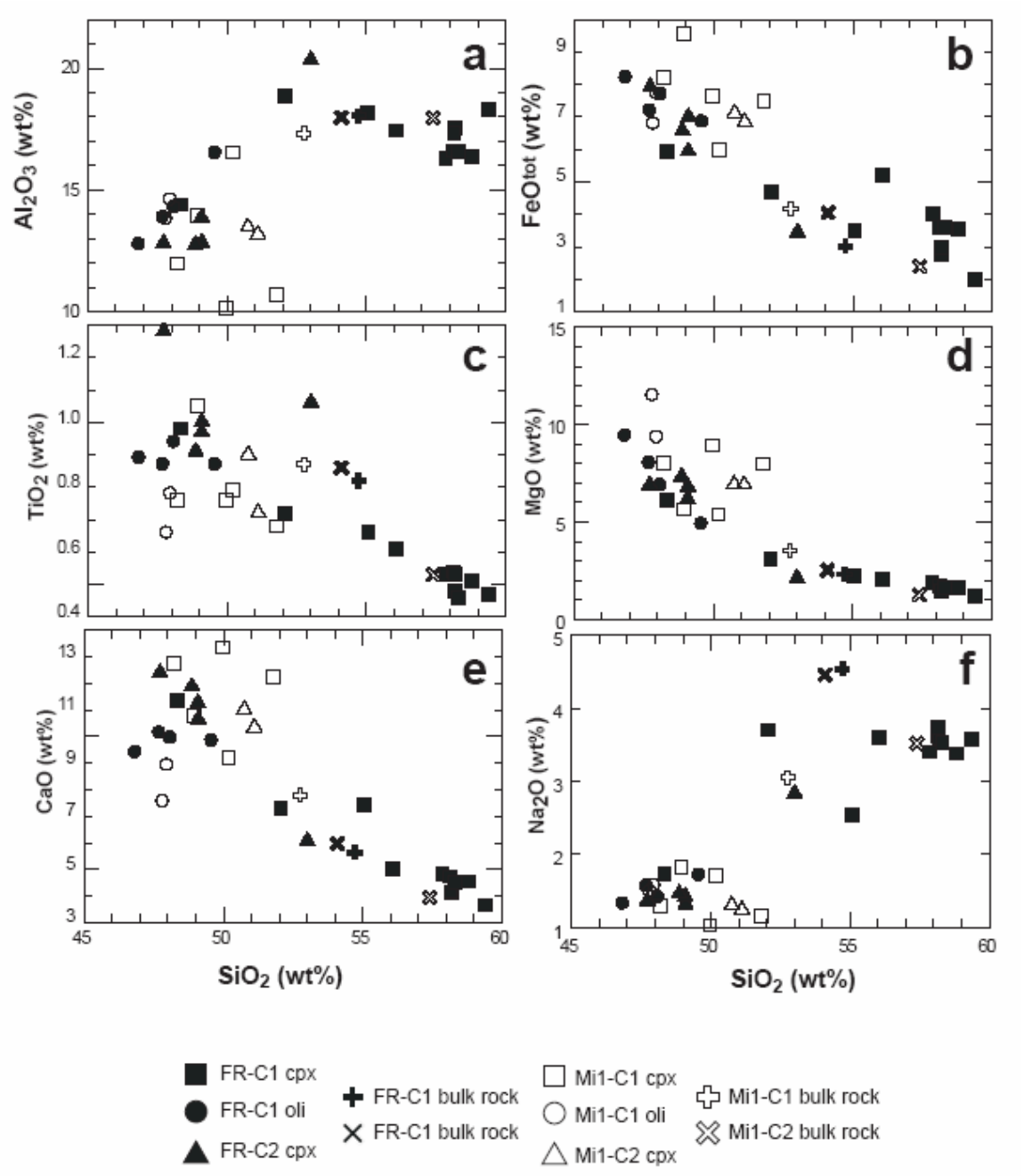

Fig. 6.4 *Harker variation diagrams for MI plotted versus SiO_2: (a). Al_2O_3; (b). CaO; (c) Na_2O.; (d). P_2O_5; (e) TiO_2; (f) FeO^{tot}.*

The volatile content of MI as a function of SiO_2 for the two eruptions are shown in Fig.6.5. The SO_2 content of MI in clinopyroxene from scoria (C1) varies between 0.04 and 0.29 wt%; and from 0.25 to 0.40 wt% for MI in olivine from the scoria (C1) and from 0.13 to 0.34 wt% for MI in clinopyroxene from the bomb (C2). For Minopoli 1 MI, SO_2 varies from 0.09 to 0.11 wt% for clinopyroxene from C1, from 0.21 to 0.34 wt% for MI in olivine from C1, and from 0.31 to 0.37 wt% for MI in clinopyroxene from C2. The SO_2 concentration decreases with increasing SiO_2, consistent with degassing during magma crystallization. MI hosted in clinopyroxene from FR-C1 shows little variation in S content as a function of SiO_2. One Minopoli 1 MI containing approximately 48 wt.% SiO_2 and 0.91 wt% SO_2 falls well outside the range of all other values. This data point was not discarded because it represents the average of two nearly identical analyses on the same MI.

Decreasing P_2O_5 with increasing SiO_2 (Fig. 6.5b) is consistent with apatite crystallization during magma evolution. No systematic variation in F is observable for the two samples (Fig. 6.5c).

Chlorine abundance (Fig. 6.5d) in the Fondo Riccio MI ranges from 0.32 to 0.72 wt % in MI in clinopyroxene from the scoria (mean of 0.54 wt%), whereas Cl shows much less variation in MI in clinopyroxene from the bomb sample (CF-FR-C2) (between 0.42 and 0.57 wt % with a mean of 0.49 wt%) and in MI in olivine from CF-FR-C1 sample (between 0.42 and 0.47 wt % with a mean of 0.44 wt %). Minopoli 1 MI show a smaller variation in Cl content compared to Fondo Riccio. Cl varies from 0.34 to 0.2 wt% in MI in clinopyroxenes from Mi1-C1 (mean 0.27 wt%), 0.43±0.01 wt% for MI in olivine from Mi1-C1 and from 0.39 to 0.42 wt.% for MI in clinopyroxene from Mi1-C2. These results suggest that the magma that generated the Fondo Riccio scoria phenocrysts was not affected by Cl loss. The Cl content is slightly higher in more evolved MI than in less evolved MI for Fondo Riccio samples (Fig. 6.5d), whereas such a trend is not observed for Minopoli 1 MI.

The average H_2O content, measured by EMPA, is consistent with the H_2O obtained by SIMS (Fig.6.6). In general, less evolved MI have higher concentrations of water and Fondo Riccio MI are enriched in H_2O compared to

Minopoli 1 MI (even though the concentrations overlap). This may explain the more explosive character of the Fondo Riccio eruption compared to the Minopoli 1 eruption.

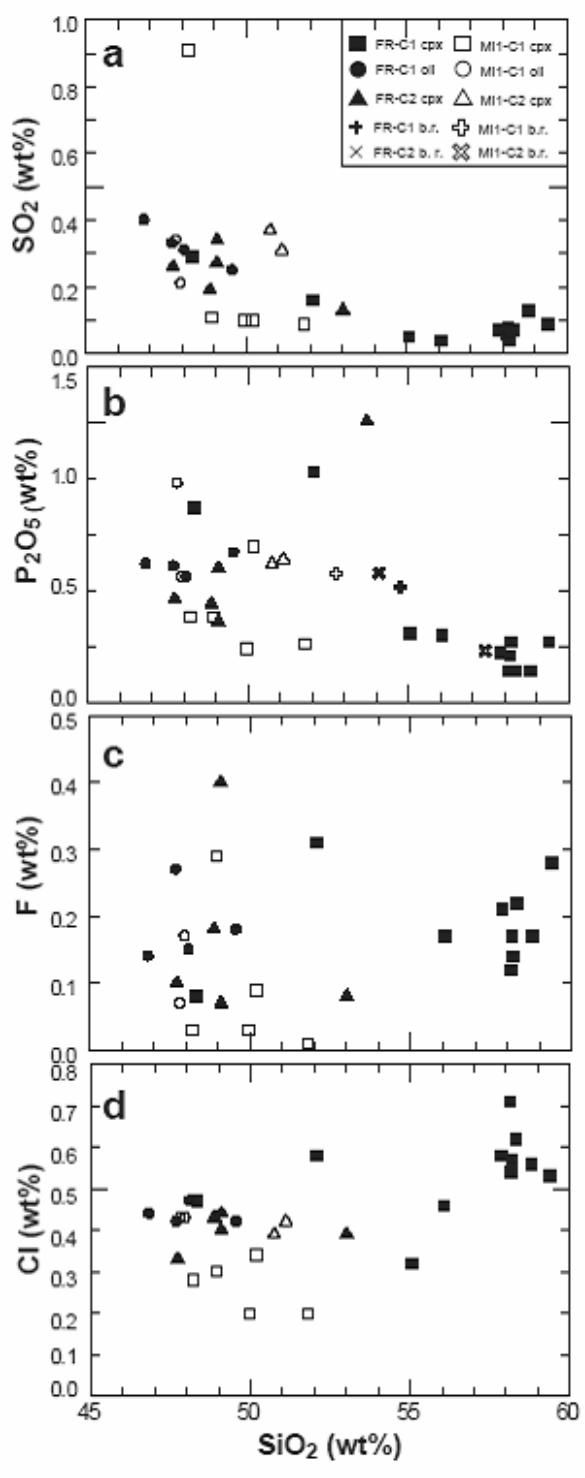

Fig 6.5 *Volatile concentrations in MI from Fondo Riccio and Minopoli 1 plotted versus SiO_2 concentration.*

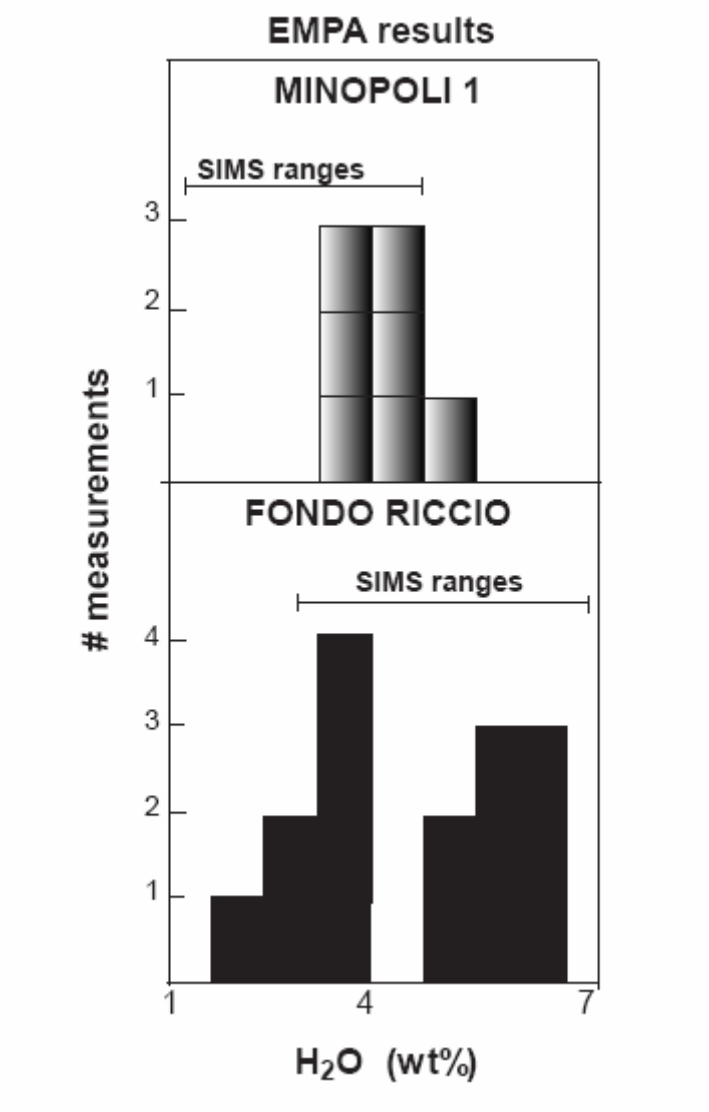

Fig. 6.6 *Water contents of MI obtained by EMPA and SIMS.*

In order to better understand the origin of the magma that fed these two eruptions, trace element systematics have been examined. Compositions of MI from both eruptions have B and Be concentrations that fall close to the B/Be = 4 line that divides rocks that originate in volcanic arc environments and those that are sourced in an ocean island volcanic setting (Fig. 6.7).

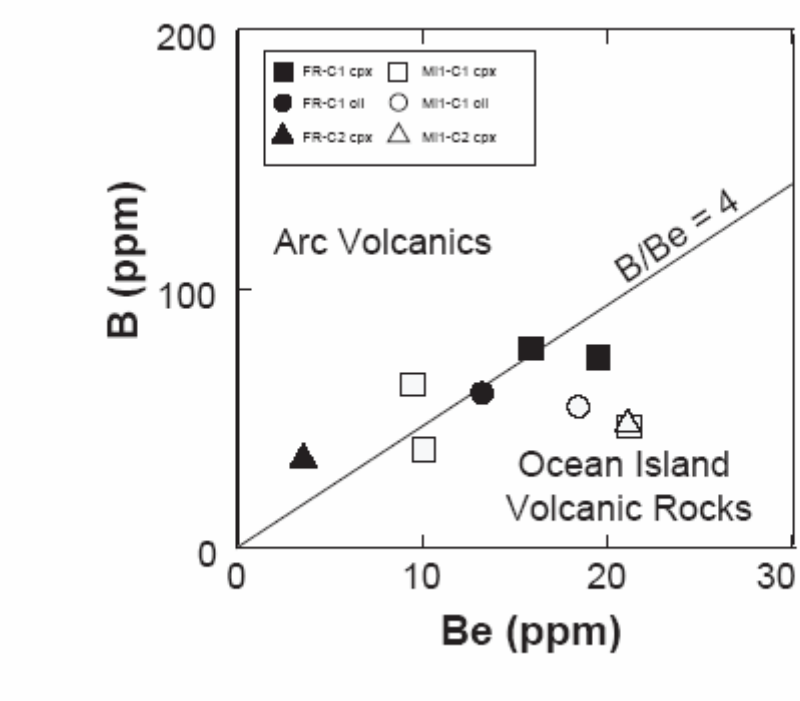

Fig. 6.7 *Relationship between B and Be for Fondo Riccio and Minopoli 1 MI. The diagonal line corresponds to B/Be = 4 and divides arc volcanic magmas from ocean island volcanic magmas. Both samples fall along the boundary line, suggesting a mixed arc volcanic and ocean island origin. Two data points for samples Mi1-C1-p6 M2 and FR-C1-o4 M1 have not been plotted.*

Rb versus Y+Nb systematics of MI straddle the boundary between rocks associated with "within plate" volcanism and those generated in volcanic arc settings (Fig. 6.8). Y/Nb versus Zr/Nb systematics of MI are consistent with magmas generated in the upper continental crust, but also point towards the island arc environment (Fig. 6.9). An upper continental crust origin for the MI is also suggested by the Sr, Rb, Th, Nb, Ce, Zr, Sm, Y and Yb spider diagram (Pearce, 1984) (Fig.6.10).

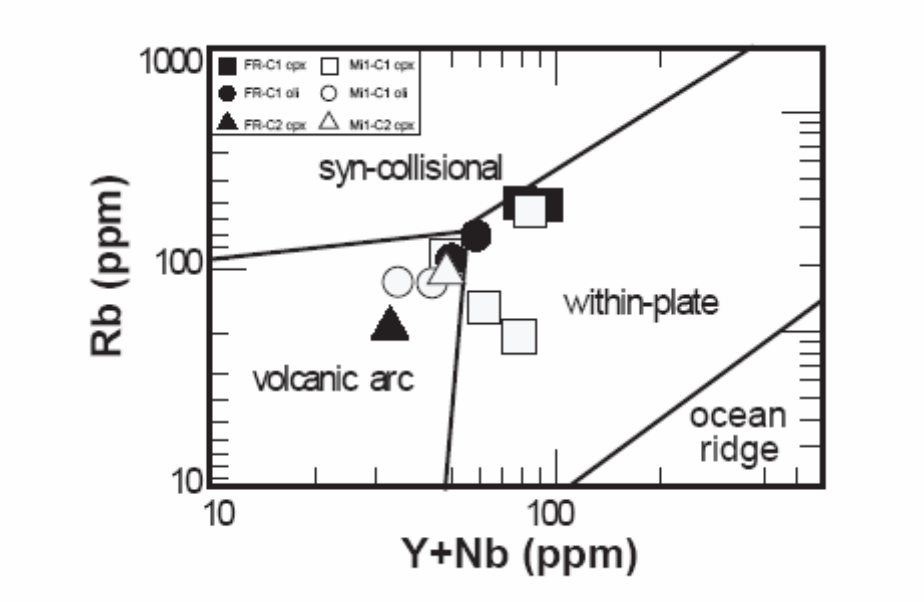

Fig. 6.8 *Relationship between Rb and Y+Nb for Fondo Riccio and Minopoli 1 MI. MI compositions are near the boundary between the volcanic arc and "within plate" fields, suggesting a mixed magma source (see also Fig.1 in Piochi et al., 2005).*

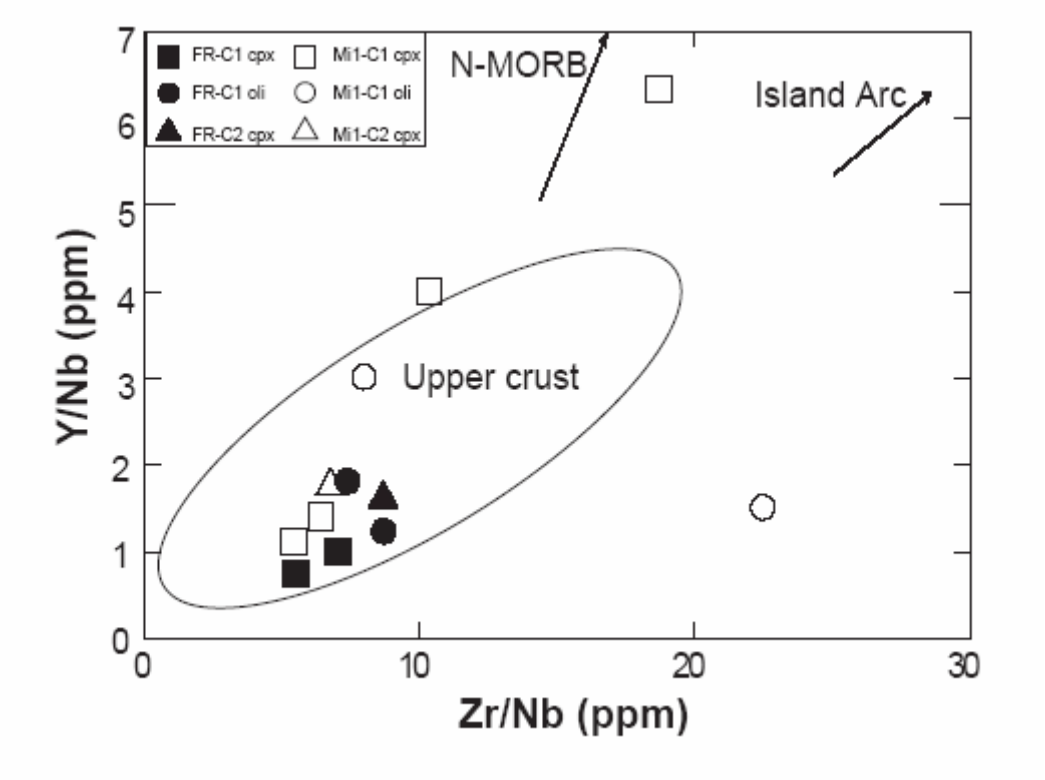

Fig. 6.9 *Relationship between Y/Nb and Zr/Nb for Fondo Riccio and Minopoli 1 MI. Compositions of MI from both samples suggest an upper crustal magma source.*

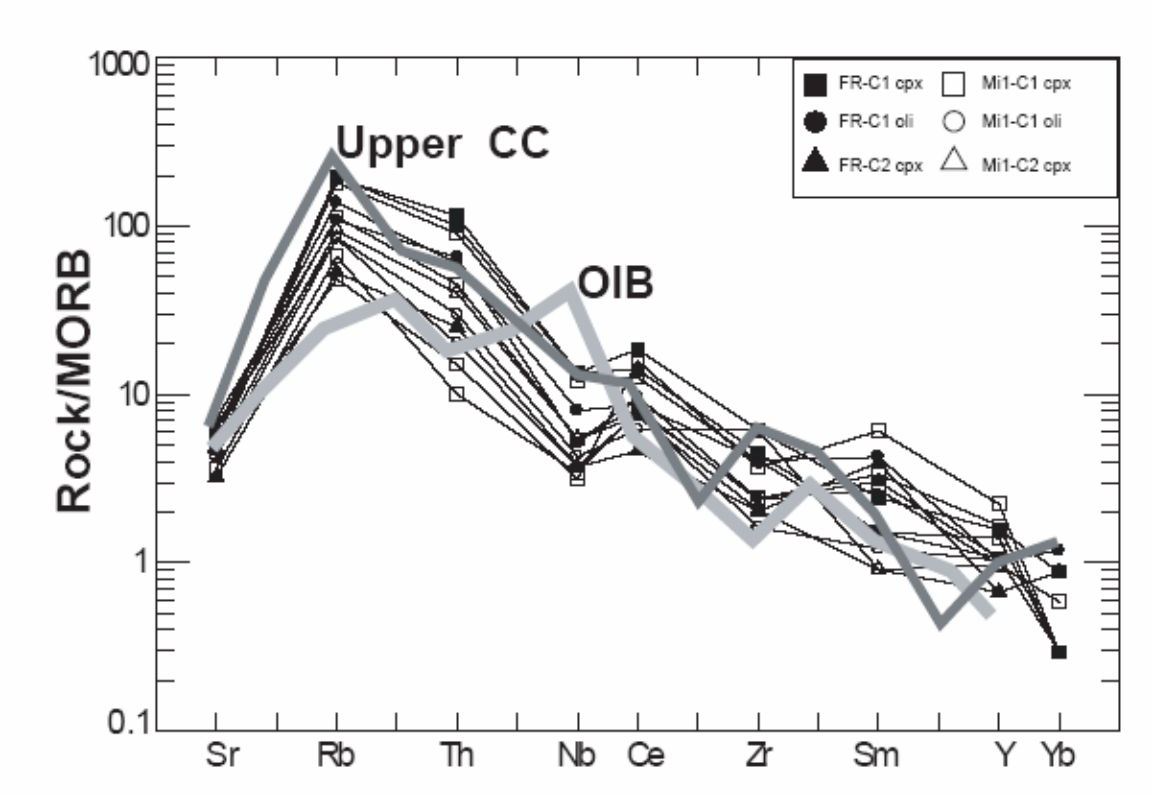

Fig. 6.10 *Spider diagram for Fondo Riccio and Minopoli 1 MI (Pearce, 1983). The heavier lines show the upper continental crust (Upper CC) and the oceanic island basalt (OIB) trends.*

The relationship between Rb and Cs for MI from Somma-Vesuvius (SV) and the Campanian Ignimbrite (CI) (shaded areas) from Webster et al., 2003 are compared with MI from this study in Fig. 6.11. The data suggest that Fondo Riccio and Minopoli 1 eruptive products were more likely generated from a magma similar to that which fed Somma Vesuvius rather than that which produced the Campanian Ignimbrite rocks.

The trace element data presented above are consistent with the tectonic setting of the Neapolitan area, and with the possible involvement of slab-derived fluids, as suggested by Piochi et al. (2005).

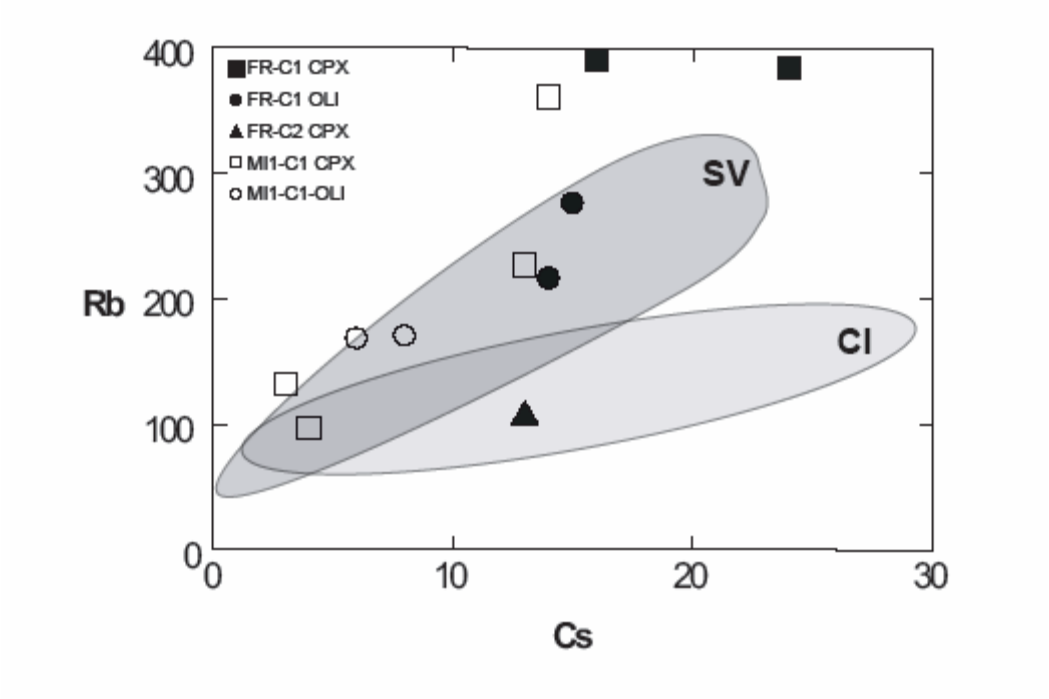

Fig. 6.11 *Relationship between Rb and Cs for Fondo Riccio and Minopoli 1 MI. The data suggest that the feeding mechanism of these two eruptions is more similar to the Somma-Vesuvius (SV) magma source than the Campanian Ignimbrite source.*

Cap 6

CONCLUSIONS

MI from Fondo Riccio and Minopoli 1 show systematic variations in composition compared to the bulk-rock compositions. Major and trace element composition of MI are consistent with an evolving magma chamber in which olivine and clinopyroxenes are crystallizing. The composition of MI in olivine from Fondo Riccio scoria (CF-FR-C1) is similar to MI in clinopyroxene from the bomb (CF-FR-C2). Except for clinopyroxene in Fondo Riccio C1, MI are generally less evolved than the corresponding host rock. Major and trace elements in Fondo Riccio MI show a wider variation compared to those in Minopoli 1 MI. This could be interpreted to indicate that the Fondo Riccio magma residence time was longer compared to the Minopoli 1 magma. Na_2O enrichment in the Fondo Riccio bulk rock represents the effects of hydrothermal activity in the volcanic system before and during the explosive eruptions (see, De Vivo and Lima, in press).

The concentration of SO_2 and H_2O is higher in less evolved MI, whereas Cl is higher in more evolved MI. F shows no obvious variation as a function of SiO_2. The generally higher volatile contents of Fondo Riccio MI are consistent with the more explosive character of this eruption compared to Minopoli 1. Trace element data suggest a combination of arc volcanic and upper continental crust magma as the source for the Fondo Riccio and Minopoli 1 eruptions. Major and trace element systematics suggest that these two eruptions, which occurred at

different times, were sourced from a single batch of magma that has evolved with time. The smaller range in compositions of the Minopoli 1 MI compared to the Fondo Riccio samples suggest a shorter residence time for Minopoli compared to Fondo Riccio magma.

REFERENCES

Anderson A.T., 1974. Chlorine, sulfur and water in magmas and oceans. Geol. Soc. Am. Bull., 85, 1485-1492

Anderson A.T., 1976. Magma mixing: Petrological process and volcanological tool. J. Volcanol. Geotherm. Res., 1, 3-33.

Anderson A.T., 2003. An introduction to melt (glass ± crystals) inclusions. In "Fluid Inclusions. Analysis and Interpretations". Min. Assoc. Canada, vol 32, pp374

Barberi F., Cassano E., La Torre P. and Sbrana A., 1991. Structural evolution of Campi Flegrei Caldera in light of volcanological and geophysical data. J. Volcanol. Geotherm. Res., 48 (1/2), 33-49

Burnham C.W., 1979. The importance of volatile constituents. In "The evolution of the igneous rocks; 50th anniversary perspective". Princeton University Press, 439-482.

Carroll M. R., Holloway J.R., 1994 Volatiles in magma. Mineral. Soc. Am. Rev. Mineral., 30

Clocchiatti R., 1975. Les inclusions vitreuses des cristaux de quartz, Etude optique, thermooptique et chemique, Applications geologiques. Soc.Geol.France, Memoires, New Series, 122, 96 pp.

Cundari A., Fergusson A.K., 1982. Significance of the pyroxene chemistry from leucite-bearing rocks and related assemblages. Tschermaks. Mineral. Petrogr. Mitt., 30, 189-204

Danyushevsky L.V., Della Pasqua F.N., Sokolov S., 2000. Re-equilibration of melt inclusions trapped by magnesian olivine phenocrysts from subduction-related magmas: petrological implications. Contrib. Mineral. Petrol., 138, 68-83

D'Antonio M., Civetta L., Di Girolamo P., 1999. Mantle source heterogeneity in the Campanian Region (South Italy) as inferred from geochemical and isotopic features of mafic volcanic rocks with shoshonitic affinity. Mineral Petrol, 67, 163-192

D'Argenio, B., T. Pescatore, and P. Scandone (1973), Schema geologico dell'Appennino Meridionale (Campania e Lucania), in Moderne Vedute della Geologia dell'Appennino, p. 183, Accad. Nazl. dei Lincei, Roma, Italy.

Deino A. L., Orsi G., de Vita S., Piochi M. 2004 The age of the Neapolitan Yellow Tuff caldera-forming eruption (Campi Flegrei caldera-Italy) assessed by $^{40}Ar/^{39}Ar$ dating method. J. Volcanol. Geotherm. Res., 133, 157-170

De Vivo B., Rolandi G., Gans P.B., Calvert A., Bohrson W.A., Spera F.J. and Belkin H.E., 2001. New constraints on the pyroclastic eruptive history of the Campanian volcanic Plain (Italy). Mineralogy and Petrology, 73, 121-143.

De Vivo B., Lima A. and Webster J. D., 2005. Volatiles in magmatic-volcanic systems. Elements, 1, 19-24.

De Vivo B. and Lima A. (in press). A hydrothermal model for ground movements (bradyseism) at Campi Flegrei, Italy. In: De Vivo B. (Edt), "Volcanisn in the Campania Plain: Vesuvius, Campi Flegrei and Ignimbrites". Developments in Volcanology 9, Elsevier.

Di Girolamo P., Ghiara M.R., Lirer L., Munno R., Rolandi G., Stanzione D., 1984. Vulcanologia e Petrologia dei Campi Flegrei. Boll Soc Geol It, 103, 349-413Di Vito M.A., Lirer L., Mastrolorenzo G., Rolandi G., 1987 The 1538 Monte Nuovo eruption (Campi Flegrei, Italy). Bull Volc, 49, no.4, 608-615

Di Vito M.A., Isaia R., Orsi G., Southon J., D'Antonio M, de Vita S., Pappalardo L., Piochi M., 1999. Volcanic and deformation history of the Campi Flegrei caldera in the past 12 ka. J Volcanol Geotherm Res, 91, 221-246

Doglioni, C. (1991), A proposal for kinematic modeling of W dipping subductions. Possible applications to the Tyrrhenian-Apennines system, Terra Nova, 3, 426–434.

Fedele L., Bodnar R.J., DeVivo B. and Tracy R.J., 2003. Melt inclusion geochemistry and computer modeling of trachyte petrogenesis at Ponza, Italy. Chemical Geology, 194, 81-104.

Frezzotti M.L., 2001. Silicate-melt inclusions in magmatic rocks: application to petrology. Lithos 55, 273–299.

Gvirtzman Z. and Nur A. (2001). Residual topography, lithospheric structure and sunken slabs in the central Mediterranean. Earth Planet. Sci. LetT. 187, pp 117-130

Hippolyte J.C., Angelier J., and Roure F. (1994). A major geodynamic change revealed by Quaternary stress patterns in the Southern Apennines. Tectonophysics, 230, 199–210.

Ippolito, F., D'Argenio B., Pescatore T., and Scandone P. (1975). Structural-stratigraphic units and tectonic framework of Southern Appennines. In Geology of Italy, edited by C. Squyres, pp. 317–328, Lybian Soc. of Earth Sci. Press, Libyan Arab Republic, Tripoli.

Le Bas M.J., Le Maitre R.W., Streckeisen A., Zanettin B., 1986. A chemical classification of volcanic rocks based on the total alkali-silica diagram. J Petrol, 27, 745-750

Lima A., 2000. Experimental study in silicate melt inclusions in clinopyroxene phenocrysts from Roccamorfina lavas (Italy) Mineral and Petrol, 70, 199-220

Lima A., De Vivo B., Fedele L. and Sintoni M.F. (in press). Geochemical variations between the 79 AD and 1944 AD Mt. Somma-Vesuvius volcanic products: constraints on the evolution of the hydrothermal system based on fluid and melt inclusions. Chem. Geol. (this volume).

Lowenstern J.B., 1994. Dissolved volatile concentrations in ore-forming magma. Geology, 22, 893-896.

Marianelli P., Metrich N., Sbrana A. 1999. Shallow and deep reservoir involved in magma supply of the 1944 eruption of Vesuvius. Bull. Volc., 61, 48-63.

Meletti C., Patacca E., and Scandone P. (2000). Construction of a seismotectonic model: The case of Italy, Pure Appl. Geophys., 157, 11–35.

Morimoto N. 1988. Nomenclature of pyroxenes. Mineral. Mag., 52, p 535-550.

Orsi G., de Vita S. and Di Vito M., 1996. The restless, resurgent Campi Flegrei nested caldera (Italy): constraints on its evolution and configuration. J. Volcanol. Geotherm. Res., 74, 179-214.

Pappalardo L., Civetta L., D'Antonio M., Deino A.L., Di Vito M.A., Orsi G., Carandente A., de Vita S., Isaia R., Piochi M., 1999. Chemical and isotopical evolution of the Phlegraean magmatic system before the Campanian Ignimbrite (37 ka) and the Neapolitan Yellow Tuff (12 ka) eruptions. J Volcanol Geotherm Res, 91, 141-166

Pappalardo L., Piochi M., D'Antonio M., Civetta L., Petrini R., 2002. Evidence for multi-stage magmatic evolution during the past 60 ka at Campi Flegrei (Italy) deduced from Sr, Nd and Pb isotope data. J. Petrol., 43, 1415-1434

Pearce J.A., Harris B.W., Tindle A.G. (1984) Trace element discrimination diagrams for the tectonic interpretation of granitic rocks. J. Petrol., 25, 956-983

Peccerillo A. (1999). Multiple mantle metasomatism in central-southern Italy: Geochemical effects, timing and geodynamic implications, Geology, 27, 315–318.

Piochi M., Bruno P.P., De Astis G. (2005) Relative roles of rifting tectonics and magma ascent processes: Inferences from geophysical, structural, volcanological, and geochemical data for the Neapolitan volcanic region (southern Italy). Geochemistry, Geophysics, Geosystems, 6, n.7

Piromallo, C., and Morelli A. (1997). Imaging the Mediterranean upper mantle by P-wave travel time tomography, Ann. Geophys., 40, 963–979.

Roedder E., 1979. “Origin and significance of magmatic inclusions”, Bull. Mineral., 102 pp. 487-510

Roedder E., 1984. “Fluid inclusions”, Reviews Mineral.12, Mineral. Soc. Am., Washington D.C., 644 pp.

Rolandi G., Bellucci F., Heizler M.T., Belkin H.E. and De Vivo B., 2003. Tectonic controls on the genesis of ignimbrites from the Campanian Volcanic Zone, southern Italy. Mineralogy and Petrology, 79, 3 - 31.

Rosi M. and Sbrana A., 1987. Phlegrean Fields. CNR, Quaderni de "La Ricerca Scientifica", 114, 1-175.

Scandone P. (1979). Origin of the Tyrrhenian Sea and Calabrian Arc. Boll. Soc. Geol. Ital., 98, 27–34.

Selvaggi G., and Amato A. (1992). Subcrustal earthquakes in the Northern Apennines (Italy): Evidence for a still active subduction?. Geophys. Res. Lett., 19, 2127–2130.

Selvaggi, G., and Chiarabba G. (1995). Seismicity and P-wave velocity image of the southern Tyrrhenian subduction zone. Geophys. J. Int., 121, 818–826.

Serri, G., Innocenti F., and Manetti P. (1993). Geochemical and petrological evidence of the subduction of delaminated Adriatic continental lithosphere in the genesis of the Neogene- Quaternary magmatism of central Italy. Tectonophysics, 223, 117–147.

Shimizu N., Hart S.R., 1982. Application of the ion probe to geochemistry and cosmochemistry. Ann. Rev. Earth Planet. Sci., 10, 483-526

Sobolev A.V., Kamenetsky V.S., Metrich N., Clocchiatti R., Koronova N.N., Devirts A.L., Ustinov V.I., 1990. Volatile regime and crystallization conditions in Etna hawaiite lavas. Geochem. Internat., 1990, 53-65

Sobolev A.V., 1996. Melt inclusions in minerals as a source of principle petrological information. Petrology, 4, 209-220

Sobolev A.V., Slutskii A.B., 1984. Composition and crystallization conditions of the initial melt of the Siberian meimechites in relation to the general problem of ultrabasic magmas. Sov. Geol. And Geophys., 25, 93-104

Student J. J., Bodnar R. J, 2004. Silicate melt inclusions in porphyry copper deposits: Identification and homogenization behavior. Canadian Mineralogist, 42, 1563-1600.

Thomas J.B., Bodnar R.J., 2002. A technique for mounting and polishing melt inclusions in small (>1 mm) crystals. Am. Min., vol.87, n.10, 1505-1508

Thomas J.B., Bodnar R.J., Shimizu N., Sinha A.K., 2002. Determination of zircon/melt trace element partition coefficients from SIMS analysis of melt inclusions in zircon. Geochimica et Cosmochimica Acta, 66, 2887-2902.

Tonarini S., Leeman W.P., Civetta L., D'Antonio M., Ferrara G., Necco A. 2004 B/Nb and $\delta^{11}B$ systematics in the Phlegraean volcanic district, Italy. J Volcanol Geotherm Res, 133, 123-139.

Veksler, I. V., 2004. Liquid immiscibility and its role at magmatic-hydrothermal transition: a summary of experimental studies. Geoch. Geol., 210, 7-31

Wallace P.J., 2005 Volatiles in subduction zone magmas; concentrations and fluxes based on melt inclusion and volcanic gas data. J.Volcanol.Geotherm.Res. 140, 1-3, 217-240

Webster J. D., Burt D.M., Aguillon R. A., 1996. Volatile and lithophile trace-element geochemistry of heterogeneous Mexican tin rhyolite magmas deduced from compositions of melt inclusions. Geochim. Cosmochim. Acta, 60, 3267-3283

Webster J. D., Raia F., De Vivo B., Rolandi G., 2001. The behavior of chlorine and sulfur during differentiation of the Mt. Somma –Vesuvius magmatic system. Mineral. Petrol., 73, 177-201.

Webster J.D., Raia F., Tappen C., De Vivo B. (2003). Pre eruptive geochemistry of the ignimbrite-forming magmas of the Campanian Volcanic Zone, Southern Italy, determined from silicate melt inclusions. Mineral. Petrol., 79, 99-125